國立交通大學

影像與生醫光電研究所

碩士論文

利用自發脈衝光引起光注入鎖模之二段式邊射型雷射高頻特性研究

Monolithic Two-Section Self-Pulsation Edge Emitting Laser With Injection Locking Technique

研究生：林智偉

指導教授：郭浩中 教授

盧廷昌 教授

中華民國一百年七月

利用自發脈衝光引起光注入鎖模之二段式邊射型雷射高頻特性研究

Monolithic Two-Section Self-Pulsation Edge Emitting Laser With Injection Locking Technique

研 究 生：林智偉　　Student：Chih-Wei Lin

指導教授：郭浩中　　Advisor：Hao-Chung Kuo

盧廷昌　　Tien-Chang Lu

國 立 交 通 大 學

影像與生醫光電研究所

碩 士 論 文

A Thesis

Submitted to Institute of Imaging and Biomedical Photonics

National Chiao Tung University

in partial Fulfillment of the Requirements

for the Degree of

Master

in

Imaging and Biomedical Photonics

July 2011

Tainan, Taiwan, Republic of China

中華民國一百年七月

利用自發回饋引起光注入鎖模之二段式可調式雷射

學生：林智偉　　指導教授：郭浩中
盧廷昌

國立交通大學影像與生醫光電研究所碩士班

摘　　要

本論文中我們研究利用回饋引起光注入鎖模的二段式可調式雷射特性，發光波長為 1.55 微米，我們使兩顆緊鄰的相同的雷射元件中央位置準確地利用聚焦離子束與電子束蝕刻出具有特定寬度深度的空氣柱，此雷射一出光端面為高反射層而另一端面為抗反射層，我們藉由共振腔光場強度的模擬結果可知主要由空氣柱的深度變化導致由主雷射的共振腔產生的雷射光注入到副雷射共振腔的注入比例不同，此外，主副雷射之間的電流分佈也隨著空氣柱的深度有所不同。我們基於光注入鎖模理論，在一個穩定的光注入鎖模範圍內，顯示出分別在有外部注入光與無外部注入光源的情況下做相對雜訊的量測與模擬，我們觀察到在有外部注入光的情況下，雷射共振腔的共振頻率可以大幅提升。理論上若使得主雷射的光注入比例越大，則共振頻率峰值可增加至 10 GHz 以上，另外利用此技術可使得相對強度雜訊能夠有效的降低，在本論文中將由特定空氣柱深度的條件設定以及鎖模情況下，改變主雷射的注入光比例使得相對強度雜訊峰值能夠至少達至 20 GHz。由此技術可使雷射大幅增加頻寬，頻譜分析與探討將在本論文中進行研究與討論。

Monolithic Two-Section Self-Pulsation Edge Emitting Laser With Injection Locking Technique

Student：Chih-Wei Lin　　Advisors：Dr. Hao-Chung Kuo

Dr. Tien-Chang Lu

Institute of Imaging and Biomedical Photonics

National Chiao Tung University

ABSTRACT

In this thesis,we study the characteristics of the 1.55 μm two-section self-feedfack laser with injection-locking technique.We fabricate an air gap with a specific width and depth in the middle of the two single-mode laser side by side with the focus ion beam system. The laser device has an high-reflection facet and an anti-reflection one on the other side. From the wave intensity simulation, we know that the injection ratio from the master laser (ML) to the slave laser (SL) will differ at different depths. Besides, the current distribution in the two-section cavity will also differ because of the different depths.

Based on the optical injection-locking theory, we present the device structure about 1.55μm two-section edge emitting laser、the relative intensity noise (RIN) measurement of the device with light injection and without light injection, and the simulation results of RIN spectrum .We can observe that the resonance frequency increase largely under a external injection light condition. Theoretically if we increase the injection ratio, the resonance frequency can be up to 10 GHz at least, and relative intensity noise can reduce effectively. In this thesis fixing some gap depths, we change the injection ratio from ML, and we can enhance the RF frequency up to 20 GHz at least under injection-locking condition. With the technique, we can increase the laser modulation bandwidth.

誌　　謝

首先必須感謝指導教授郭浩中與盧廷昌老師半導體雷射實驗室給予我豐沛的實驗資源，讓我無需擔心實驗事宜，然而最感謝的是林建中老師的對我實驗內容的不厭其煩的親自督導與討論，每當遇到瓶頸時總給予適時的幫助以及給我正確的方向解決問題，祝老師們研究順利，身體健康。

其次要感謝的是陳智弘老師與林俊廷老師實驗室對於我的實驗所需的軟硬體部分全力支援，以及感謝何俊鴻博士生以及趙明義同學的居中協調與實驗儀器教育訓練；感謝程育人老師實驗室的成員，也給予我適當的實驗協助，讓我的實驗能夠順利進行。

感謝獸皇學長在我碩一下的時候教我實驗操作、還有珣文學姐、鏡學學長與我在模擬上的討論、博孝學長的 DBR 鍍膜協助，感謝阿國、SGG、90 哥、Just、幼齒、肉哥、家齊、翌臻、瑋婷、KaKa、峰瑜、冠霖、大寶、小杜、Joseph、板弟、阿伯、信助、奇穎、威麟等等，以及台南校區光電學院第一屆的同學們，有了你們的陪伴使我的碩士生涯多采多姿。

最後，感謝我的父母給予我全力的支持，讓我求學生涯無後顧之憂，讓我能夠完成學業。

林智偉 2011/07/31 於交通大學

CONTENTS

List of Tables

List of Figures

Chapter .1 Introduction

1.1 Light sources on optical communication system

Modern communication system would be efficient, cost-effective, operating at high data rates. The system could use radio links between portable and mobile user equipment ,for instance , notebook computers and mobile telephones to ensure flexibility and convenient services. For the purpose of providing high capacity and for using the available frequency band efficiently the cell size should be small. Ultrahigh-speed clock recovery is an essential element for future optical communications. To achieve optical retiming, reshaping, and reamplification (3R regeneration), clock recovery at the aggregate line rate is required. Moreover, The optical fibers transmit the modulated radio carriers to the radio nodes allowing the radio node to be very simple. It may transmit high data rate baseband digital signal as part of the local LAN at the same time.

	F-P	**DFB**	**VCSEL**
Lasing mode	Edge-emitting	Edge-emitting	Surface-emitting
Wavelength	1310,1550nm	1310,1550nm	850,980,1310,1550nm
Price(US)	100~200	200~300	20,100
Rate(bps)	622M,2.5G	2.5G,10G	155M,1.25G

Table1.Comparision of different lasing modes of laser devices

For the subcarrier multiplexed optical application great dynamic range and high linearity are required for the optical devices to have good system performance and avoid channel crosstalk [1]. The type of light source suitable for optical communication depends not only on the communication distance but also on the bandwidth requirement. For long-haul and wide bandwidth communications invariably laser diodes are used because of their narrow linewidth and high output power and ease of coupling into single-mode fiber.[2]

The semiconductor lasers that lase in the wavelength range 1.3-1.55μm are irreplaceable sources of coherent optical communication lines, frequency-division multiplexing systems[3].Moreover, the absorption wavelength of many molecules lies near 1.55μm. The most common laser-diode configuration is the distributed feedback(DFB) laser,which uses grating layer adjacent to the active region acting as a distributed reflector that substitutes for the mirrors of a Fairy-Perot laser. Edge-emitting lasers offer narrow spectral widths, critical for the efficient operation of 1.3 and 1.5μm wavelength-division-multiplexed(WDM) optical communication systems[2].

1.2 Introduction of the multisection laser

Self-pulsation DFB lasers are a desirable source for the generation of millimeter-wave carriers over fiber and can be broadly used in a WDM configuration for wireless networks operating at 40 GHz[4].Besides, self-pulsating DFB lasers have many promising applications in future optical communication network, for all-optical clock recovery especially, a key function in all-optical 3R regeneration[5]. Self-pulsating DFB laser diodes with multiple DFB regions were fabricated for this purpose. Generally speaking, such multisection DFB lasers are divided into the two-section type and the three-section type, and three different SP mechanisms have been proposed, including spatial hole burning, dispersive self-Q-switching and beating-type oscillations [6].There are several methods of tuning the wavelength of a semiconductor laser. Electrical tuning is one of the most simple and reliable methods. In most cases a multisection laser is used for this purpose. Recently, a theoretical investigation showed that the variation in the ridge width of a two section DFB laser leads to a slight wavelength difference of the lasing mode in each DFB section, and in turn gives rise to the beating between the two lasing modes.[7] This process varies electron and hole densities that under the influence of the electric field are accelerated and generate a THz wave equal to the difference frequency between the two optical modes.[8] It is attractive to develop a THz signal source more compact and cost effective to fabricate.One possible means is to use a dual-mode semiconductor laser with two modes simultaneously emitting at two different wavelengths from a single or combined laser cavity [9]. The use of the dual-mode laser has the advantage of being free of optical alignment issues since there is no need to align two laser beams. There are many optical cavity approaches have been demonstrated that achieve simultaneous two-mode generation from a monolithic system [10].

1.3 Motivation

A considerable amount of literature has been published on multisection lasers utilizing the injection locking mechanism.Injection locking technique using master and slaver laser is promising for generating millimeter-wave because it is simple to implement and gives high tunability.However,the experiment setups used to achieve sideband injection locking often require two or more light source-a master laser and slave laser,or a master laser and two slave laser.In this thesis,we successfully fabricated novel two-section lasers,first,we experimentally demonstrated optical generation of millimeter-wave using monolithic injection locking of a two section DFB laser without any external optical element.And we hope that we can at least enhance the relaxation oscillation frequency and push the relative intensity noise peak up to 10 GHz by optical injection-locking technique. We would detail the whole story in the following sections.

References

[1]Tamas Marozdk*, Eszter Udvary* “Vertical Cavity Surface Emitting Lasers in Radio Over Fiber Applications”

[2]B.E.A.Saleh,M.C.Teich “Fundamental Of Photonics Second Edition”

[3] N. A. Pikhtin, A. Yu. Leshko, A. V. Lyutetski , V. B. Khalfin, N. V. Shuvalova,Yu. V. Il’in, and I. S. Tarasov Two-section InGaAsP/InP Fabry-Perot laser with a 12 nm tuning range, Pis’ma Zh. Tekh. Fiz. 23, 10–15 ~March 26, 1997

[4] Al-Mumin M, Mao W, Li Y and Li G 2001” 40 GHz millimetre-wave link based on two-section gain-coupled DFB Lasers” *Electron. Lett.* 37 915–6

[5] Bornholdt C, Sartorius B, Schelbase S, Mohrle M and Bauer S 2000”Self-pulsating DFB laser for all-optical clock recovery at 40 Gbit s^{-1} *Electron. Lett.* 36 327–8

[6] Wenzel H, Bandelow U, Wunsche H J and Rehberg J 1996”Mechanisms of fast self pulsations in two-section DFB lasers” *IEEE J. Quantum Electron.* 32 69–78

[7] H. Hillmer, A. Grabmaier, S. Hansmann, H. -L. Zhu, H. Burkhard, and K. Mazagi, IEEE J. of Selected Topics in Quant. Electr. 1, 356 (1995).

[8] E. R. Brown, “THz generation by photomixing in ultrafast photoconductors,” Int. J. High Speed Electron. Syst. 13(2), 497–545 (2003).

[9] C.-L. Wang, and C.-L. Pan, “Tunable multiterahertz beat signal generation from a two-wavelength laser-diode array,” Opt. Lett. 20(11), 1292–1294 (1995).

[10]Wan Q, Sun C-Z, Xiong B, Wang J and Luo A novel multisection distributed feedback laser with varied ridge width for self-pulsation generation *Chin. Phys. Lett.* 23 2753–5 , (2006)

Chapter 2 Theory

2.1 Optical Injection Locking

In 1980 Kobayashi and Kimura used GaAs lasers to demonstrate the injection locking experimental results. [1] Using two devices with close wavelength is necessary. In 2005 Lukas Chrostowski, Xiaoxue Zhao and Connnie J Chang-Hasnain used 1.55μm VCSEL to demonstrate the resonance frequency enhanced from 7GHz up to ~50GHz [2]. The technique is that one laser the master laser (ML) is external light source to inject photons in another laser the slave laser (SL). The resonant frequency enhancement might result from the external light injecting into the slave laser as a cavity increasing the photons in the slave laser. Using the technique has some advantages, such as side-mode suppression ratio(SMSR), enhancement of the relaxation oscillation, improvement of the nonlinear characteristic and chip frequency and so forth. It makes direct modulation more adequate for many applications.

The direct modulation of semiconductor lasers can be used for transmitting subcarrier-multiplexed signals at low cost of using injection locking to improve the nonlinear characteristic.[3] The resonance frequency enhancement by using the injection locking technique means that we will have much larger bandwidth can be used in optical communication. The technique can adequately improve the dynamic operation characteristic so that injection-locked lasers is a practicable way to use for future networks.

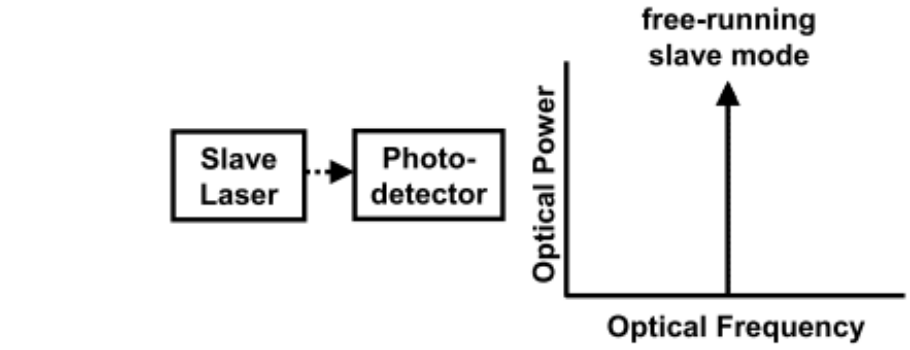

(a)

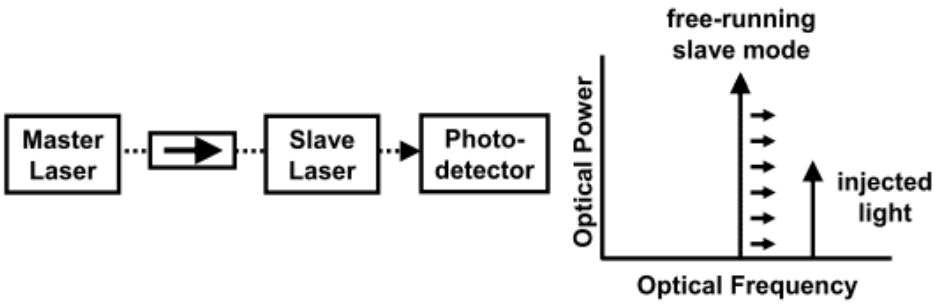

(b)

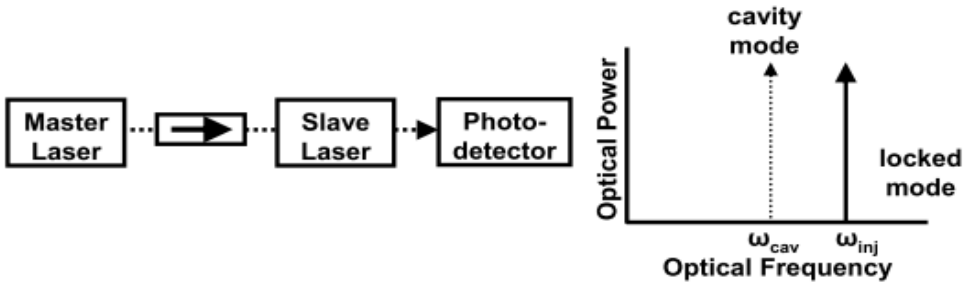

(c)

Figure 2.1.1 Optical Injection-Locking On Semiconductor Laser

2.2 Theoretical Model

The dynamics of injection-locked lasers are simulated by rate equations which couple the temporal variations of the amplitude, the phase and the number of carriers of the slave laser:

$$\frac{dA(t)}{dt} = \frac{1}{2} g[N(t) - N_{th}]A(t) + \kappa A_{inj} \cos\phi(t) \quad \text{Eq 2.2.1}$$

$$\frac{d\phi(t)}{dt} = \frac{\alpha}{2} g[N(t) - N_{th}] - \kappa \frac{A_{inj}}{A(t)} \sin\phi(t) - 2\pi\Delta f \quad \text{Eq 2.2.2}$$

$$\frac{dN(t)}{dt} = J - \gamma_N N(t) - \{\gamma_p + g[N(t) - N_{th}]\}A^2(t) \quad \text{Eq 2.2.3}$$

where A(t) is the field amplitude, defined as A^2 (t)=S(t), where S(t) is the photon number.φ (t) is the phase difference between the temporal laser field of the slave laser and master laser. N(t) is the carrier number and J is the injection current. N_{th} is the threshold carrier number, g is the linear gain coefficient, γ_P is the photon decay rate, κ (= 1/τ in) is coupling coefficient, τ_{in} is the cavity round-trip time of the slave laser, α is the linewidth enhancement factor of the slave laser, and γ_N is the carrier decay rate. N_{th} also defines the carrier number at the onset of lasing, and contains both transparency carrier number and photon loss rate: $g_N = N_{tr} + \gamma_p/g$.

By applying small signal linear approximation and stability analysis to the above rate equations [4, 5, 6], the injection locking range, $\Delta\omega_L$,and locking stabilities can be derived and plotted as following:

$$-\sqrt{1+\alpha^2}\,\kappa\left(\frac{A_{inj}}{A_0}\right) < \Delta\omega_L < \kappa\left(\frac{A_{inj}}{A_0}\right) \quad \text{Eq 2.2.4}$$

,where A_0 is the stationary amplitude of the slave laser under optical injection. The regions of injection locking stability are shown as a function of injection locking parameters in Figure 2.1.2. Equation 2.2.4 and Figure 2.1.2 illustrate that stronger optical injection broadens the stable injection locking range.

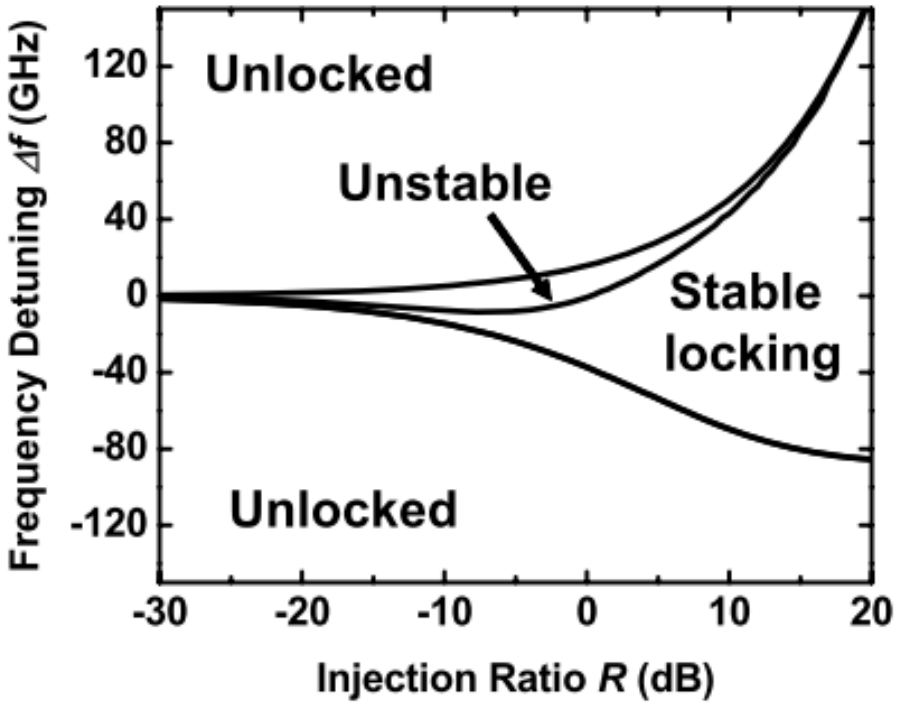

Figure 2.1.2 Injection locking stability as a function of injection ratio R and frequency detuning Δf.

2.3 Linewidth enhancement factor

In 1981, Fleming and Mooradian demonstrated the linewidth of a semiconductor laser and found the linewidth is different from Schawlow-Townes predicted. They were unable to explain the result [7]. In 1982, Charles H. Henry wrote a paper about the theory of the linewidth of semiconductor [8]. In general, the phase of the optical field fluctuation to influence the laser linewidth. The fluctuations are due to the spontaneous emission.Linewidth enhancement factor(α) is the deviation of the imaginary part and real part of the refraction index.

$$\alpha \equiv \frac{\Delta n_r}{\Delta n_i} = \frac{\partial n_r / \partial n}{\partial n_i / \partial n}$$

Linewidth enhancement factor is attributed to the change in refractive index with carrier density. Due to the Kramers-Kronig relations, we can find the change in the imaginary part of the susceptibility will change the real part of the susceptibility.

The refractive:

$$n = n_r - jn_i$$

The value of the linewidth enhancement factor is dependent on the dimension of the quantization. The complex refractive index changes by the carrier density. We can observer from the follower formulas [9].

$$n_r(\omega) = \frac{1}{2\varepsilon_0 n} \sum \int < R_{ch}^2 > \frac{g_{ch}(f_c - f_v)(E_{ch} - \hbar\omega)}{(E_{ch} - \hbar\omega)^2 + (\frac{\hbar}{\tau_{in}})^2} dE_{ch}$$

$$n_i(\omega) = \frac{1}{2\varepsilon_0 n} \sum \int < R_{ch}^2 > \frac{g_{ch}(f_c - f_v)\hbar\omega/\tau_{in}}{(E_{ch} - \hbar\omega)^2 + (\frac{\hbar}{\tau_{in}})^2} dE_{ch}$$

The change of the linewidth enhancement factor with different quantization dimension alters the term of g_{ch}. g_{ch} is the density-of-states of the electron-hole pair. It is expresses by the step and delta functions, for a quantum well and quantum box. The change in the imaginary part of the susceptibility (gain or loss) will be influence by a corresponding change in its real part (refractive index) through the Kramers-Kronig relations. A symmetrical gain curve will lead to the dispersion curve of the refractive index has a zero at the frequency corresponding to the gain peak[10]. Large value will result in chirp under direct modulation in optical fiber communication.There are several methods to measure the linewidth enhancement factor, such as RF-modulation measurement, the interferometric measurement, the amplified spontaneous emission (ASE) method and using the locking region measurement [11]

2.4 Simulation theory

We start with a wave-guiding structure and define the z-direction when the direction of propagation. The basic equation is the Maxwell equations. However, we would like to go further and obtain a set of equations directly usable in solving the system. Under the assumption of the scalar wave, the wave equation can be solved with the variable separation technique.We assume that the solution to the wave equation can be written as the product

$$E_\omega(x,y,z) = E_\omega(z)\phi_0(x,y) \qquad \text{Eq.2-1.1}$$

where ω is the optical frequency and z is the direction of the waveguide. The distribution $\phi_0(x,y)$ can be calculated effectively by other approaches for instance the effective index method or the beam propagation method.The simulation software solves the problem including all the governing semiconductor equations. The z-dependent part of the electric field satisfies the equation.

$$[\frac{\partial^2}{\partial z^2} + k^2(z)]E_\omega(z) = f_\omega(z) \qquad \text{Eq.2-1.2}$$

where $f_\omega(z)$ is the Langevin noise function because of spontaneous emission. We notice that the noise function is very important for a laser device because it is a driving force for the solution. For an isolated semiconductor laser, the physical solution for Eq. 2-1.2 would be zero if the spontaneous noise term was absent. A simple physical explanation is that the spontaneous emission noise generates or excites the photons, amplified by the the optical gain. The optical power is determined both by the spontaneous emission and the optical gain at any bias condition. The complex propagation constant k(z) contains information about the solution of the transverse and lateral dimensions, or in other words, it is calculated from the effective

index at a specific cross section in the xy-plane. The effective index and the k(z) are dependent on the frequency, material properties and the photon density ,as a result of the non-linear gain suppression.

Using Green's function in the analysis of DFB lasers was first proposed by C.H. Henry [12] and later extensively used by Tromborg [13] in deriving analytical formulas for DFB lasers. We has used the Green's function method because of its accuracy in treating spontaneous emission,and its conceptual simplicity.It is also suitable for numerical implementation.The Green's function method starts with the wave equation, 2-1.2. The objective is to obtain a compact expression for the solution to the noise driven wave equation. In the Green's functions method, the solution to Eq. 2-1.3 can be written as

$$E_{\omega}(z) = \frac{\int_0^l g(z,z')\, f_{\omega}(z')dz'}{W} \qquad \text{Eq.2-1.3}$$

where $f_{\omega}(z')$ is the local Langevin force, $g(z,z')$ the Green's function, and W the Wronskian of the wave equation. The integration is over the diode cavity length l. The Wronskian *W is a* functional *of the* distribution of the wavenumber [k(w,N(z))] in general. The interpretation of Eq.2-1.3 is very simple according to the basic principle of the Green's function method. The Green's function method says that for any linear differential equation with a driving source term, the solution can be found by decomposing the source into many smaller pieces in space. The Green's function can be written as

$$g(z,z') = Z_R(z)\cdot Z_L(z')\cdot\Theta(z-z') + Z_R(z')\cdot Z_L(z)\cdot\Theta(z'-z) \qquad \text{Eq.2-1.4}$$

Here $\Theta(z)$ is the Heaviside step function. $Z_L(z)$ is the solution to the homogeneous wave equation, which satisfies the boundary condition at the left laser

facet and internal interfaces for multi-section lasers but may not satisfy the boundary condition at the right laser facet. $Z_R(z)$ is the corresponding solution which satisfies the boundary condition at the right facet and the internal interfaces. The Wronskian can be written as

$$W = Z_L(z)\frac{d}{dz}Z_R(z) - Z_R(z)\frac{d}{dz}Z_L(z) \qquad \text{Eq.2-1.5}$$

Since $Z_L(z)$ and $Z_R(z)$ are solutions to the homogeneous wave equation, it follows from simple algebra that $\frac{dw}{dz} = 0$ in each waveguide section. This means that W is position independent.Therefore, under a particular bias condition, the Wronskian is only a function of the frequency or wavelength.

For the detailed 2D E-field distribution, we need to use a more elaborated way to simulate this problem.The basic equations used to describe the semiconductor device behavior are Poisson's equation and the current continuity equations from Maxwell's equations for electrons and holes:

$$-\nabla\left(\frac{\varepsilon_0\varepsilon_{dc}}{q}\times\nabla V\right) = -n + p + N_D(1-f_D) - N_A f_A + \sum_j N_{tj}\left(\delta_j - f_{tj}\right) \qquad \text{Eq.2-1.6}$$

$$\nabla J_n - \sum_j R_n^{tj} - R_{sp} - R_{st} - R_{au} = \frac{\partial n}{\partial t} + N_D\frac{\partial f_D}{\partial t} \qquad \text{Eq.2-1.7}$$

$$\nabla J_p + \sum_j R_p^{tj} + R_{sp} + R_{st} + R_{au} = -\frac{\partial p}{\partial t} + N_A\frac{\partial f_A}{\partial t} \qquad \text{Eq.2-1.8}$$

, where V is electrical potential, n and p are electron concentration and hole concentration, N_D and N_A are doping of shallow donors(D) and shallow acceptors(A),f_D and f_A are occupancy of donor (D) and acceptor(A) levels, N_{tj} is density of j th deep trap,f_{tj} is occupancy of the j th deep trap level , J_n and J_p are current flux densities,R_{ntj} and R_{ptj} are electron and hole recombination rate for

quantum well, R_{sp} is spontaneous recombination rate, R_{st} is stimulated recombination rate, R_{au} is auger recombination rate. By solving the above equation sets, we could calculate more precisely the field distribution within the cavity.

2.5 Couple-Wave Equations

As was discussed in the previous section, the problem has been reduced to solving for the Green's function and the corresponding Wronskian. These in turn require the knowledge of the solution of the homogeneous wave equation

$$[\frac{\partial^2}{\partial z^2} + k^2(z)]E_\omega(z) = 0 \qquad \text{Eq2-2.1}$$

where k(z) is the wavenumber of the waveguide given by

$$k^2 = n^2 \frac{\omega^2}{c_0^2} \qquad \text{Eq2-2.2}$$

c_0 is the speed of light in vacuum and n is the refractive index. The wave number may depend directly on z due to the grating structure or variation in the material composition and indirectly through the carrier density and photon density variations along the waveguide.

In DFB and DBR lasers, corrugations are made along the wave guides which introduce coupling between forward and backward waves. The purpose is to perturb the propagation constant $k(z)$ to achieve desirable scattering effects to the propagating waves. In a laser with a grating of period L_g, its effective refractive index can be written as

$$n = \tilde{n} + 2(\Delta n)\cos(\frac{2\pi}{L_g(z)}z + \Omega) \qquad \text{Eq 2-2.3}$$

where we consider the general case that the grating period may vary as a function of position. $\tilde{n}$ denotes the slow varying part of the complex index and $2(\Delta n)$ is the magnitude of the index variation which is again a complex quantity. We define a reference wave number which is usually set to the Bragg wave number in simple grating structures at threshold condition such that

$$\beta_0 = \frac{\pi}{< L_g >} \qquad \text{Eq 2-2.4}$$

where $\langle\ \rangle$ used to denote the average grating period. β_0 is a constant independent of the frequency and injection conditions. In general, we can assume that the change in the grating period is smooth and write the following expansion,

$$\frac{\pi}{< L_g >} = \beta_0 + \beta_{ch}(z) \qquad \text{Eq 2-2.5}$$

where $\Delta\beta_{ch}(z)$ is caused by some form of chirp grating variation of grating period. Based on Eq. 2-2.3, we re-write the wave number as

$$k = \beta_0 + \Delta\tilde{k} + 2\kappa\cos[2(\beta_0 + \Delta\beta_{ch})z] + j\Omega] \qquad \text{Eq 2-2.6}$$

$$= \beta_0 + \Delta\tilde{k} + \kappa e^{2j(\beta_0+\Delta\beta_{ch})z]+j\Omega} + \kappa e^{-2j(\beta_0+\Delta\beta_{ch})z]-j\Omega} \qquad \text{Eq 2-2.7}$$

where

$$\Delta\tilde{k} = \tilde{n}\frac{\omega}{c_0} - \beta_0 \qquad \text{Eq 2-2.8}$$

and

$$\kappa = \Delta n\frac{\omega}{c_0} \qquad \text{Eq 2-2.9}$$

Since only the optical frequencies close to the Bragg condition are considered, the second term in Eq. 2-2.7 is small compared with β_0. Similarly we assume that the coupling coefficient κ is much smaller than β_0. In the following derivation, we will neglect higher order terms of $\Delta\tilde{k}$ and κ. We propose a trial solution of the form:

$$E_z = R(z)e^{-j\beta_0 z} + L(z)e^{j\beta_0 z} \qquad \text{Eq 2-2.10}$$

where $L(z)$ and $R(z)$ are used to denote the slow varying amplitudes of waves going left and right, respectively. We substitute it into the wave equation to get the following algebra:

$$-\beta_0^2[R(z)e^{-j\beta_0 z} + L(z)e^{j\beta_0 z}] - 2j\beta_0[(\frac{\partial R(z)}{\partial z})e^{-j\beta_0 z} + (\frac{\partial L(z)}{\partial z})e^{j\beta_0 z}]$$
$$+(\frac{\partial^2 R(z)}{\partial^2 z})e^{-j\beta_0 z} + (\frac{\partial^2 L(z)}{\partial^2 z})e^{j\beta_0 z} + k(R(z)e^{-j\beta_0 z} + L(z)e^{j\beta_0 z}) = 0 \qquad \text{Eq 2-2.11}$$

Treating $\Delta\tilde{k}$ and κ as small quantities, we expand the wave number k^2 as follows.

$$k^2 = \beta_0^2 + 2\beta(\Delta\tilde{k} + \kappa e^{2j(\beta_0+\Delta\beta_{ch})z]+j\Omega} + \kappa e^{-2j(\beta_0+\Delta\beta_{ch})z]-j\Omega}) \qquad \text{Eq 2-2.12}$$

+higher order terms.

which is then substituted into Eq. 2-2.11. To simplify the notation, we introduce a slow varying function

$$\Omega_g(z) = 2\Delta\beta_{ch}(z)z + \Omega \qquad \text{Eq 2-2.13}$$

We further assume that the wave amplitude is a slow varying function of z and neglect the second derivatives involving $(\frac{\partial^2 R(z)}{\partial^2 z})$ and $(\frac{\partial^2 L(z)}{\partial^2 z})$.After the terms involving β_0^2 are canceled, we are left with the following equation.

$$-2j\beta_0[(\frac{\partial^2 R(z)}{\partial^2 z})e^{-j\beta_0 z}+(\frac{\partial^2 L(z)}{\partial^2 z})e^{j\beta_0 z}]$$
$$+2\beta_0(\Delta\tilde{k}+\kappa e^{2j\beta_0 z+j\Omega_g}+\kappa e^{-2j\beta_0 z-j\Omega_g})(R(z)e^{-j\beta_0 z}+L(z)e^{j\beta_0 z})=0 \quad \text{Eq 2-2.14}$$

Since $R(z)$ and $L(z)$ are independent functions, this equation makes sense only when terms with the same propagation factor sum up to zero. In other words, the terms with $e^{-j\beta_0 Z}$ and $e^{j\beta_0 Z}$ must sum up zero, respectively. Collecting these terms, we find

$$-2j\beta_0(\frac{\partial R(z)}{\partial z})+2\beta_0\Delta\tilde{k}R(z)+2\beta_0\kappa e^{-j\Omega_g z}L(z)=0 \quad \text{Eq 2-2.15}$$

$$2j\beta_0(\frac{\partial L(z)}{\partial z})+2\beta_0\Delta\tilde{k}L(z)+2\beta_0\kappa e^{j\Omega_g z}R(z)=0$$

or in matrix notation:

$$\frac{\partial}{\partial z}\begin{pmatrix}R(z)\\L(z)\end{pmatrix}=\begin{pmatrix}-j(\Delta\tilde{k}) & -j\kappa e^{-j\Omega_g}\\ j\kappa e^{j\Omega_g} & j(\Delta\tilde{k})\end{pmatrix}\begin{pmatrix}R(z)\\L(z)\end{pmatrix} \quad \text{Eq 2-2.16}$$

2.6 Theory of relative intensity noise(RIN)

RIN peak is a good show of the relaxation frequency of the device. The driving force not input current is the Langevin force (F_s, F_n and F_φ) of the field due to the spontaneous emission. The Langevin force is assumed to be irrelative white Gaussian noise [14]. The relative intensity noise (RIN) spectrum is frequency dependence. The former can be derived from the rate equations.

The intrinsic relative intensity noise(RIN) of a device is defined as

$$RIN = \frac{< \delta P(t)^2 >}{P_0^2} \qquad \text{Eq 2-3.1}$$

P_0 is the average power and $\delta P(t)^2$ is the mean square power fluctuation. From a small-signal analysis of the rate equations for a single-mode laser, we can derive the noise spectrum of the device. The relative intensity noise spectrum of external light injected locked device can be derived using the follow rate equations [15].

$$\frac{ds}{dt} = \frac{G_0(N - N_{th})}{1 + \varepsilon s} \cdot S - \frac{S}{\tau_p} + 2k_c\sqrt{S \cdot S_{inj}} \cdot \cos(\phi(t) - \phi_{inj}) + R_{sp} + F_s$$

$$\frac{d\phi}{dt} = \alpha \cdot \frac{G_0(N - N_{th})}{2} - 2\pi \cdot \Delta f - k_c\sqrt{\frac{S_{inj}}{S}} \cdot \sin(\phi(t) - \phi_{inj}) + R_{sp} + F_\phi$$

$$\frac{dN}{dt} = \frac{I}{q} - \frac{N}{\tau_s} - \frac{G_0(N - N_{th})}{1 + \varepsilon s} \cdot S + F_N \qquad \text{Eq 2-3.2}$$

S , ϕ and N are the photon number, the phase and the carrier number inside the slave laser cavity. G_0 is the gain coefficient, N_0 is the transparency carrier number, τ_p is the photon lifetime, τ_n is the carrier lifetime, I is the slave laser bias current, ε is the gain compression factor, and α is the linewidth enhancement factor. F_s , F_φ and F_n are the noise terms. $\Delta\omega$ is the detuning between the master and slave laser. S_{inj} is the photons injection into the slave laser. k_c is the coupling coefficient, which determined by the photon injected into the cavity-round trip time.

We based model of injection-locked rate equation is usually used to describe the interaction between photons and carriers inside a laser cavity. When an additional light source is injected into the cavity, the system preserves the general form of the original equations, but with extra terms describing the effects of the injection.

$$F_s = F_s(\omega)\cdot e^{j\omega\cdot t},\ F_\phi = F_\phi(\omega)\cdot e^{j\omega\cdot t},\ F_N = F_N(\omega)\cdot e^{j\omega\cdot t}$$

$$S = S_0 + S_1(\omega)\cdot e^{j\omega\cdot t},\ \phi = \phi_0 + \phi_1(\omega)\cdot e^{j\omega\cdot t}$$

$$N = N_0 + N_1(\omega)\cdot e^{j\omega\cdot t}\ ,\ S = S_0 + S_1(\omega)\cdot e^{j\omega\cdot t}$$

Substituting into the injection-locked rate equation

$$i\omega\cdot S_1(\omega) = \frac{G_0(N_0 - N_{tr})}{1+\varepsilon\cdot S_0}\cdot S_1(\omega)\cdot\left(1-\frac{\varepsilon\cdot S_0}{1+\varepsilon\cdot S_0}\right)+\frac{G_0 N_1(\omega)}{1+\varepsilon\cdot S_0}\cdot S_0-\frac{S_1(\omega)\cdot e^{j\omega\cdot t}}{\tau_p}$$

$$+2k_c\cdot\left(\sqrt{\frac{S_{inj}}{S_0}}\right)\cdot\frac{S_1(\omega)}{2}\cdot\cos(\phi_0-\phi_{inj})-\sqrt{S_0 S_{inj}}\sin(\phi_0-\phi_{inj})\cdot\phi_1(\omega))+F_s(\omega) \qquad \text{Eq 2-3.3}$$

For the phase part:

$$i\omega\cdot\phi_1(\omega)=\frac{\alpha\cdot G_0\cdot N_1(\omega)}{2}-k_c\left(\sqrt{\frac{S_{inj}}{S_0}}\left(-\frac{S_1(\omega)}{2}\sin(\ \phi_0-\phi_{inj})+\cos(\ \phi_0-\phi_{inj})\cdot\phi_1(\omega\ )\right)+F_\phi(\omega\ )\right) \quad \text{Eq 2-3.4}$$

Finally, for the carrier part:

$$i\omega\cdot N_1(\omega)=-\frac{N_1(\omega\ )\cdot e^{j\omega t}}{\tau_s}-\frac{G_0(N_0-N_{tr})}{1+\varepsilon\cdot S_0}\cdot S_1(\omega)\cdot\left(1-\frac{\varepsilon\cdot S_0}{1+\varepsilon\cdot S_0}\right)-\frac{G_0\cdot N_1(\omega\ )}{1+\varepsilon\cdot S_0}S_0+F_n(\omega\ ) \quad \text{Eq 2-3.5}$$

Equations (2-3.3), (2-3.4), (2-3.5) are written in matrix form:

$$A\begin{bmatrix}S_1\\ \phi_1\\ N_1\end{bmatrix}=\begin{bmatrix}F_s\\ F_\phi\\ F_N\end{bmatrix}$$

$$A=\begin{bmatrix}i\omega-\frac{G_0(N_0-N_{tr})}{1+\varepsilon\cdot S_0}\left(1-\frac{\varepsilon\cdot S_0}{1+\varepsilon\cdot S_0}\right) & 2k_c\sqrt{S_0\cdot S_{inj}}\cdot\sin(\ \phi_0-\phi_{inj}) & -\frac{G_0}{1+\varepsilon\cdot S_0}\cdot S_0\\ +\frac{1}{\tau_p}-k_c\sqrt{\frac{S_{inj}}{S_0}}\cdot\cos(\ \phi_0-\phi_{inj}) & & \\ -\frac{k_c}{2}\sqrt{\frac{S_{inj}}{S_0}}\sin(\ \phi_0-\phi_{inj}) & i\omega+k_c\sqrt{\frac{S_{inj}}{S_0}}\cdot\cos(\ \phi_0-\phi_{inj}) & -\frac{\alpha}{2}S_0\\ \frac{G_0\cdot(N_0-N_{tr})}{1+\varepsilon\cdot S_0}\left(1-\frac{\varepsilon\cdot S_0}{1+\varepsilon\cdot S_0}\right) & 0 & i\omega+\frac{G_0}{1+\varepsilon\cdot S_0}\cdot S_0+\frac{1}{\tau_s}\end{bmatrix}$$

The laser RIN

$$RIN(\omega)=\left|S_1(\omega)\right|$$

The small-signal modulation response can also be found from this system by considering I as the small signal modulation current.

$$\begin{bmatrix}S_1\\ \phi_1\\ N_1\end{bmatrix}=A^{-1}\begin{bmatrix}0\\ 0\\ I\end{bmatrix}$$

The modulation response transfer function will be

$$H(\omega) = \frac{|S_1(\omega)|}{I(\omega)}$$

The light injected into the cavity of the slave laser and depletes the carrier density. It makes the spontaneous emission rate reduced and more photons are coupled in phase into the amplified injection field. The more photons in phase and the relaxation frequency should enhance. The RIN spectrum shows that the relaxation frequency peak becomes higher with injections. At a lower injection level directly adds photons into the slave laser cavity by using more carriers, compensating the gain saturation and enhances the relaxation peaks of the slave laser. Under the stronger injections condition, the injected photons deplete the most of the available carriers, saturate the signal and decrease the relaxation peaks finally. It prevents the further improvement of the relaxation frequency.

References

[1] S. Kobayashi and T. Kimura,"Coherence on injection phase-locked AlGaAs semiconductor laser," *Electronics Letters*, vol. 16, pp. 668-670, 1980

[2] Lukas Chrostowski, Xiaoxue Zhao and Connie J. Chang-Hasnain, “50 GHz Directly-Modulated Injection-Locked 1.55 μm VCSELs,” Optical Society of America, 2005

[3] Erwin K Lau,"High-Speed Modulation of Optical Injection-Locked Semiconductor Lasers," *Electrical Engineering and Computer Sciences University of California at Berkeley*, 2006

[4] S. Mohrdiek, H.Burkhard, and H. Walter, "Chirp reduction of directly modulated semiconductor lasers at 10 Gb/s by strong CW light injection," J. Lightw. Technol., vol. 12, no. 3, pp. 418-424, Mar. 1994.

[5] R. P. Braun, G. Grosskopf, R. Meschenmoser, D. Rohde, F. Schmidt, and G. Villino,"Microwave generation for bidirectional broadband mobile communications using optical sideband injection locking," Electron. Lett., vol. 33, no. 16, pp. 1395-1396, Jul. 1997.

[6] X. Lixin, W. H. Chung, L. Y. Chan, L. F. K. Lui, P. K. A. Wai, and H. Y. Tam, "Simultaneous all-optical waveform reshaping of two 10-Gb/s signals using a single injection-locked Fabry-Perot laser diode," IEEE Photon. Technol. Lett., vol. 16, no. 6, pp. 1537-1539, Jun. 2004.

[7] M. W. Fleming and A. Mooradian, “Fundamental line broadening of single-mode(GaA1)As diode lasers,’’ *Appl. Phys. Lett.*, vol. 38, p. 511, 1981.

[8] CHARLES H. HENRY, “Theory of the Linewidth of Semiconductor Lasers,’’ *IEEE journal of quantum electronics*, vol. QE-18, no. 2, February 1982

[9] Yasunari Miyake and Masahiro Asada, “Spectral Characteristics of Linewidth

Enhancement Factor α of Multidimensional Quantum Wells, " *Japanese journal of applied physics,* vol 28 pp1280-1281, 1989

[10] MAREK OSINSKI and JENS BUUS, "Linewidth Broadening Factor in semiconductor Lasers-An Overview" *Quantum Electronics, IEEE Journal of, 1987*

[11] G. Liu, X. Jin, and S. L. Chuang,"Measurement of Linewidth Enhancement Factor of Semiconductor Lasers Using an Injection-Locking Technique" *IEEE photonics technology letters*, VOL. 13, NO. 5, MAY 2001

[12] C. H. Henry, ``Theory of spontaneous emission noise in open resonators and its application to lasers and optical amplifiers," *J. Lightwave Technol.*, LT-4, 288-297 (1986).

[13] B. Tromborg, H. Olesen, and X. Pan, ``Theory of linewidth for multi-electrode laser diodes with spatially distributed noise sources," *IEEE J. Quantum Electron.*, QE-27, 178-192 (1991).

[14] X. Jin and S. L. Chuang , "Relative intensity noise characteristics of injection-locked semiconductor lasers, "*APPLIED PHYSICS LETTERS*, vol 77, NUMBER 9 , 28 AUGUST (2000)

[15] Lukas Chrostowski, "Optical Injection Locking of Vertical Cavity Surface Emitting Lasers," Fall (2003)

Chapter 3.

Simulation Result of the Self-pulsation Laser

3.1 Background on design

In this section a single gapped FP laser diode will be introduced which forms the basis for our platform.The single gap laser is fabricated by etching into the waveguide of the FP laser diode. The gaps act as reflection centers and produce a modulation of the reflection and transmission spectra dependent on the characteristics of the slot such as gap position, gap depth to which it is etched and slot width. Even if the gap is not etched into the active regions it will still interact with the mode of the electric field of the waveguide as the mode profile is not fully confined to the active region and will expand into the surrounding cladding regions. The 1D first order electric field mode profile modeled using the finite difference time domain technique for a simple laser structure with active region depth of 1 µm, upper cladding region of 1 µm and lower cladding of 1 µm with active region refractive index of 3.55 and cladding region refractive index 3.41, which are normal values for an InGaAsP active region sandwiched between InP cladding regions, are shown below in Fig. 3.1.1.

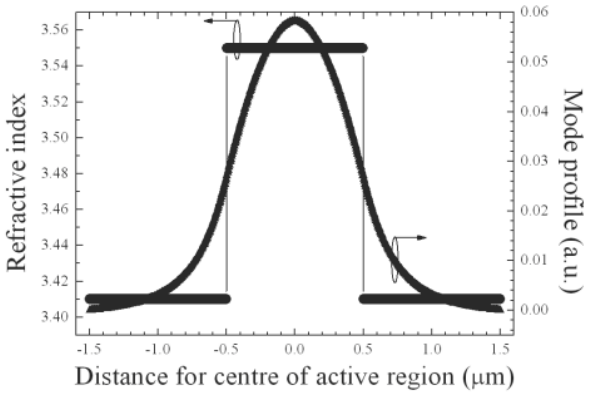

Figure. 3.1.1 Mode profile of the fundamental mode and refractive index profile through the laser structure.[1]

From Fig. 3.1.1 the fundamental mode is seen to penetrate into the cladding region so any perturbation in this area will influence the mode profile. The scattering matrix method is a easy and accurate technique which can be used to determine the reflection and transmission from gaps etched into the laser cavity.Numerous texts deal with the SMM of which is a good introduction.Of particular importance in a laser structure is the ability to determine loss using the method. This is an important advantage of the SMM over that transmission matrix method (TMM). A FP laser with one etched slot can be described as three cavities with different interface reflections and transmissions as described below in Fig 3.1.2.

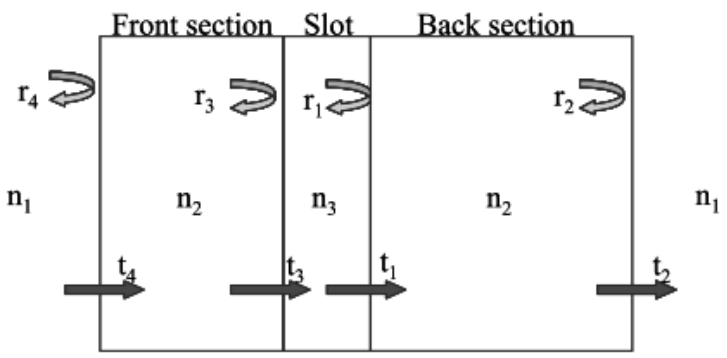

Figure 3.1.2. Schematic description of single slot laser diode.[1]

In fig. 3.1.2, n_i refers to the effective refractive index in these section of the laser structure, while r_i refers to the reflection from the interfaces as shown above. Each section can be described as a separated cavity and the total reflection and transmission is then found.The back section amplitude reflection from the left side and right side is described as

$$r_{bl} = r_1 + \frac{t_1 r_1 (-t_1) \exp\left(-2i\tilde{\beta}_b L_b\right)}{1 - r_2 (-r_1) \exp\left(-2i\tilde{\beta}_b L_b\right)}$$

and

$$r_{br} = -r_2 + \frac{t_2(-r_1)(-t_2)\exp\left(-2i\tilde{\beta}_b L_b\right)}{1-r_2(-r_1)\exp\left(-2i\tilde{\beta}_b L_b\right)}$$

respectively where β is the complex propagation constant ($\beta = \beta_{re} + i\beta_{im}$) and L_b is the back section cavity length. The back section amplitude transmission from the left side is described as

$$t_{bl} = \frac{t_1 t_2 \exp\left(-i\tilde{\beta}_b L_b\right)}{1-r_2(-r_1)\exp\left(-2i\tilde{\beta}_b L_b\right)}$$

and

$$t_{br} = t_{bl}$$

giving a power reflection and transmission is $R_{bl} = r_{bl}^2$ and $T_{br} = t_{br}^2$ respectively. The reflection and transmission of the back section and gap region is found by including the back section reflection and transmission in the SMM calculation as follows

$$r_{bl+sl} = r_3 + \frac{t_3 r_{bl}(-t_3)\exp\left(-2i\tilde{\beta}_s L_s\right)}{1-r_{bl}(-r_3)\exp\left(-2i\tilde{\beta}_s L_s\right)}$$

and

$$t_{bl+sl} = \frac{t_3 t_{bl}\exp\left(-i\tilde{\beta}_b L_b\right)}{1-r_{bl}(-r_3)\exp\left(-2i\tilde{\beta}_s L_s\right)}$$

again by a continuation of this method the reflection and transmission amplitudes for the full laser structure can be determined as

$$r_{total} = r_4 + \frac{t_4 r_{bl+sl}(-t_4)\exp\left(-2i\tilde{\beta}_f L_f\right)}{1 - r_{bl+sl}(-r_4)\exp\left(-2i\tilde{\beta}_f L_f\right)}$$

and

$$t_{total} = \frac{t_4 t_{bl+sl}\exp\left(-i\tilde{\beta}_f L_f\right)}{1 - r_{bl+sl}(-r_4)\exp\left(-2i\tilde{\beta}_f L_f\right)}$$

where the reflection and transmission from the right is found in a similar fashion to the total from the left.The calculated power reflection using an experimentally determined gain profile is shown in Fig. 3.1.3 [1]

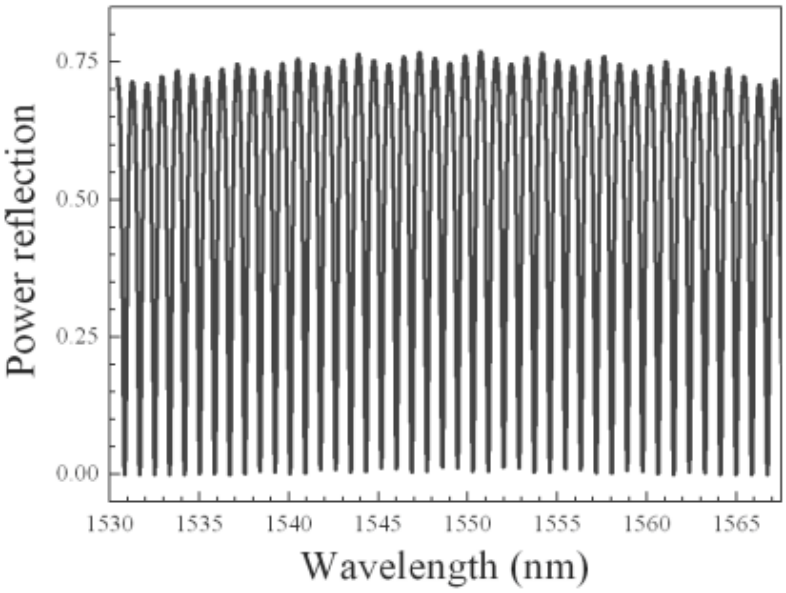

Figure 3.1.3 Calculated reflection spectrum of a single gap laser (1550 nm).

3.2 Wave intensity distribution analysis

To solve this problem, initially we took an finite difference technique [4] for the start. The variation in the third dimension is assumed to be uniform for now. When we simulate the device structure, the pumped region was indexed a little higher to mimic the optical source field. Fig. 3.2.1 shows the two dimensional field distribution. When calculating the axial field intensity, we can find out a sharp increase of confinement when the D_{gap} increases more than 2um as shown in Fig. 3.2.2.

For the detailed 2D E-field distribution, we need to use a more elaborated way to simulate this problem.The basic equations used to describe the semiconductor device behavior are Poisson's equation and the current continuity equations from Maxwell's equations for electrons and holes:

$$-\nabla\left(\frac{\varepsilon_0\varepsilon_{dc}}{q}\times\nabla V\right)=-n+p+N_D(1-f_D)-N_A f_A+\sum_j N_{tj}\left(\delta_j-f_{tj}\right)$$

$$\nabla J_n-\sum_j R_n^{tj}-R_{sp}-R_{st}-R_{au}=\frac{\partial n}{\partial t}+N_D\frac{\partial f_D}{\partial t}$$

$$\nabla J_p+\sum_j R_p^{tj}+R_{sp}+R_{st}+R_{au}=-\frac{\partial p}{\partial t}+N_A\frac{\partial f_A}{\partial t}$$

, where V is electrical potential, n and p are electron concentration and hole concentration, N_D and N_A are doping of shallow donors(D) and shallow acceptors(A),f_D and f_A are occupancy of donor (D) and acceptor(A) levels, N_{tj} is density of j th deep trap,f_{tj} is occupancy of the j th deep trap level , J_n and J_p are current flux densities,R_{ntj} and R_{ptj} are electron and hole recombination rate for quantum well, R_{sp} is spontaneous recombination rate, R_{st} is stimulated recombination rate, R_{au} is auger recombination rate.

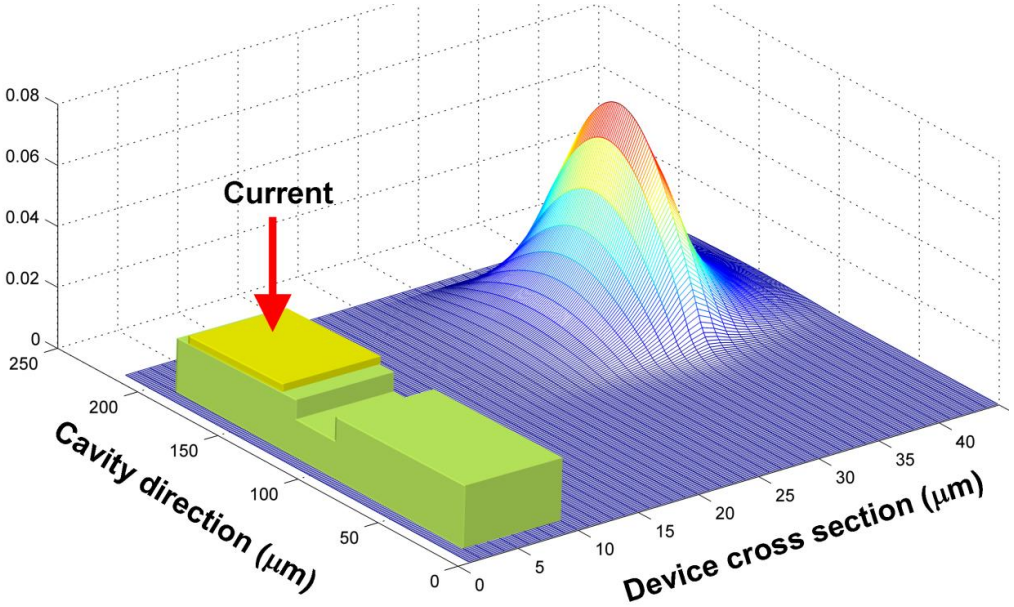

Figure 3.2.1. 2-dimensional simulation of pumped dual-section cavity

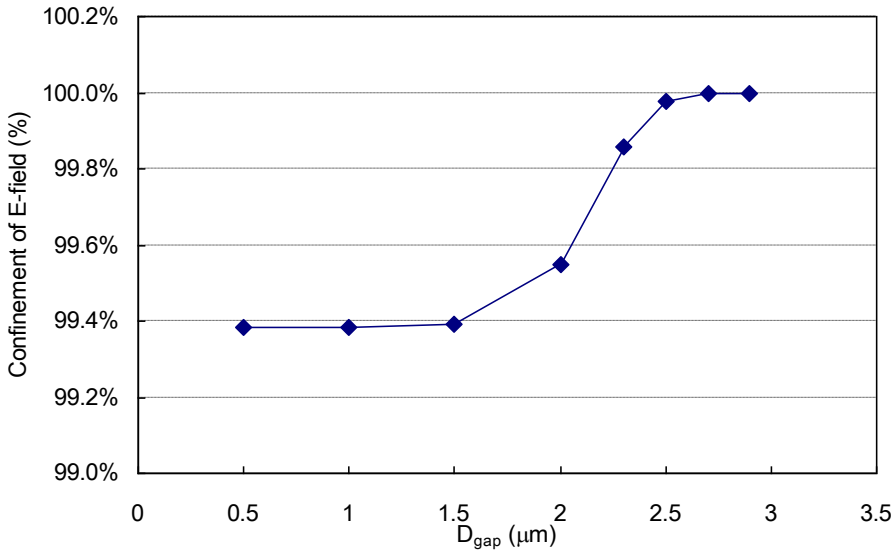

Figure 3.2.2. Calculation of confinement of E-field in the quantum well axial direction.

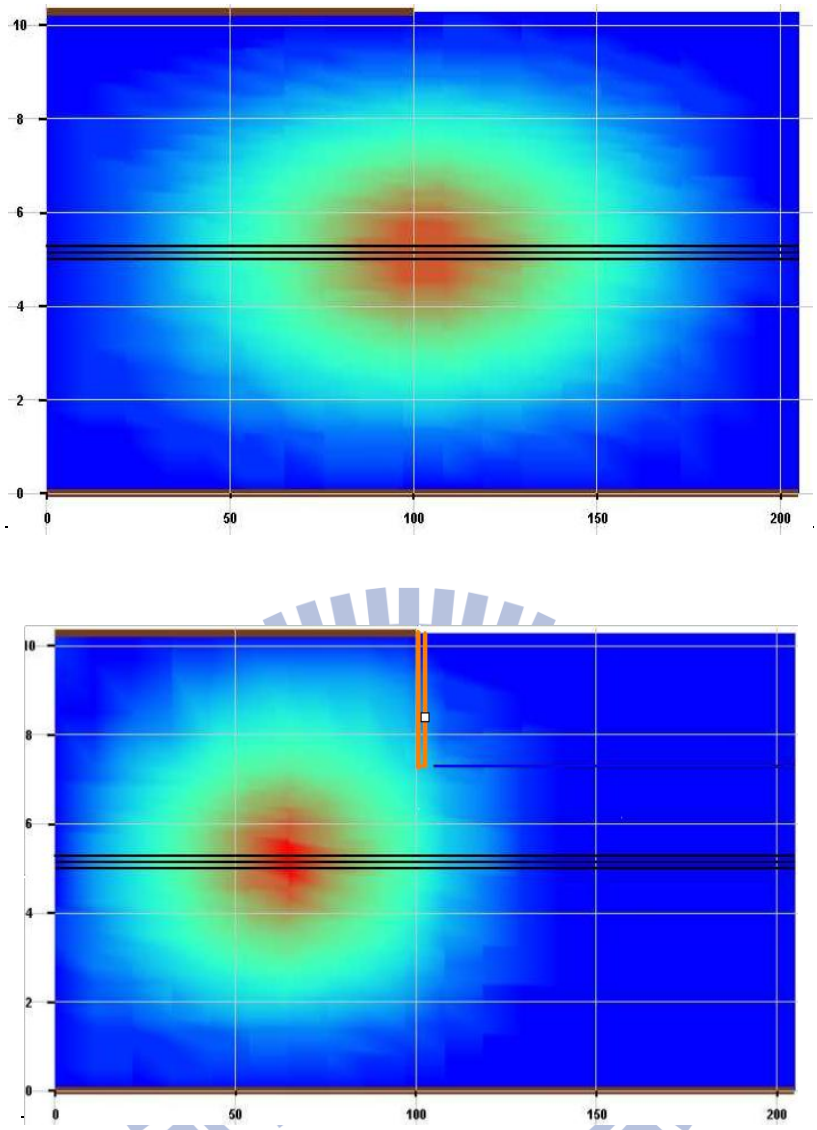

Figure 3.2.3. (a) Field distribution: W_{gap}=5μm, but with no air gap; (b) Field distribution on W_{gap}=5μm,D_{gap}=5 μm

W_{gap}	D_{gap} =1μm	D_{gap} =3μm	D_{gap} =5μm
2μm	50.3%	90.1%	90.4%
3μm	49.7%	90.8%	93%
5μm	55.4%	93.4%	94%

Table 2. Field intensity ratio on the pumped cavity

By solving the above equation sets, we could calculate more precisely the field distribution within the cavity. First of all, we started the simulation under R_1=R_2=0.32 and I_2 off .We focus now on the wave intensity distribution with an air gap of different depths and widths.Figure 3.2.3(a) shows the E-field distribution without any gap. Figure 3.2.3(b) shows that the wave intensity is re-distributed when the depth of the air gap is increased to 5μm, the field is hardly penetrated into the right section. We calculated the wave intensity distribution ratio of the pumped cavity versus the overall field intensity shown at the Table 1. When there is no depth on the chip, the left field intensity is about 50.3% at width of gap is 2μm and is 55.4% at the width of the air gap is 5μm. There is little difference of intensity ratio between the two cases. However, once we start increase Dgap, and widen Wgap, the obvious partition of field intensity can be observed. The detailed 2 dimensional calculation is summarized in table 1. As we could see, the influences of the air gap is profound. Most of the excited E-field is confined in the pumped region, however, some of them will leak into the other un-pumped (or cold) cavity. This leakage is the source of interference of the other section of laser and usually we don't know, to what extent, this leakage will disturbing the operation of the other laser unless we can quantify it. Using this method, we can estimate the possible feedback or coupling between multiple sections of semiconductor lasers.

3.3 Two-Section Laser dynamic characteristics with different slot depth

3.3.1 L-I curve

When we put a air slot in the middle section of the two-section laser, the basic performances such as laser power, current distribution or leakage current , which could be influenced to what extent by different $D_{gap.}$Therefore,we have to do some simulation and measurement about the basic performances after the focus ion beams process.

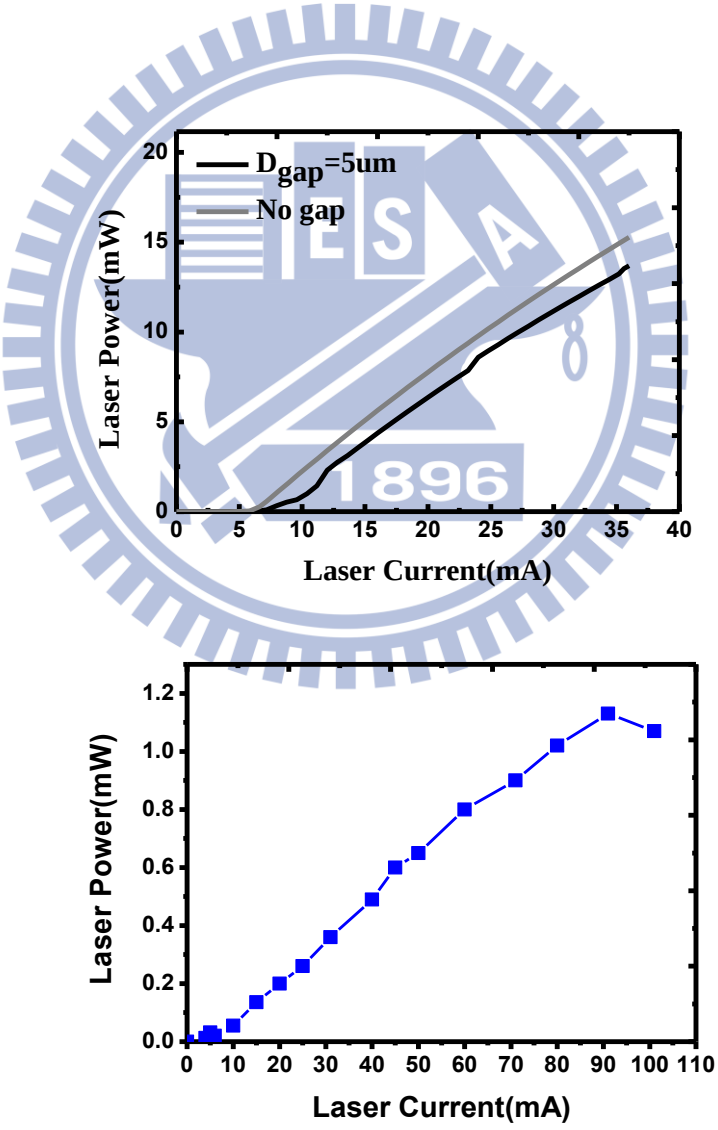

Figure 3.3.1.L-I curve (a) simulation results with air gap D_{gap}=5um and with no gap(b) measurement result with D_{gap}=5um

The figure 3.3.1(a) shows the L-I simulation result of un-FIB laser, which is normal average performance on the two-section laser. The figure 3.3.1(b) shows the L-I measurement result under different bias current. In addition, the threshold current is matches, while the power is decrease at 91mA due to large bias current which leads to the spatial hole burning.

If we etch the laser to D_{gap}=5um,the threshold current could increase and the laser power decrease a little. Hower,etching to the active layer, we can see not only the threshold current will increase more but also the laser power will fall down sharply. We could have the most moderate D_{gap} to etch the two section laser.

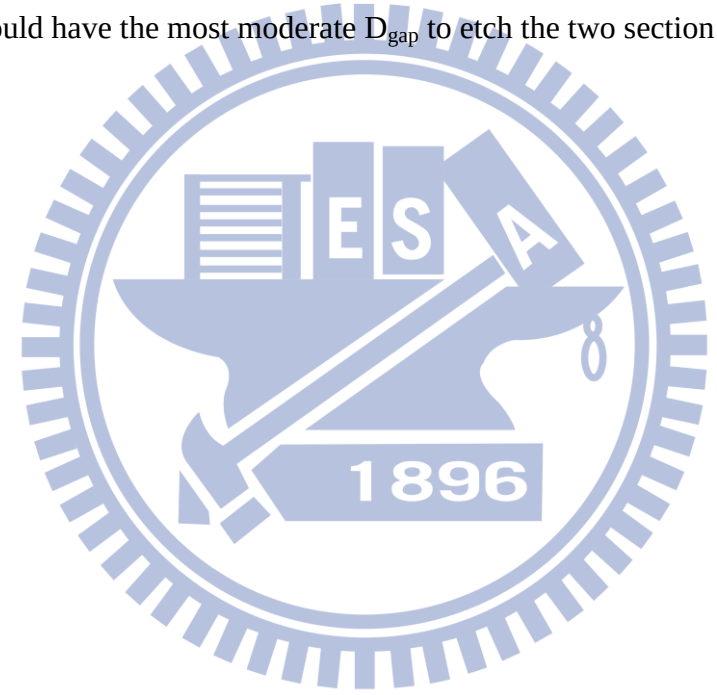

3.3.2 Leakage current

Our monolithic two-section laser is not composed of two independent lasers.However,the two sections have a common laser grating and an optical cavity originally. After the FIB etching process, the monolithic laser has two asymmetric laser cavities, but it still have common active layers.So,the other characteristic what we want to know is the laser current distribution after FIB process.

Because the pumped cavity current could leak through the cold cavity, it might give rise to some influence on cold cavity. From the figure 3.3.2(a), we can see that some leakage current inject through the active layer on the cold cavity with an air gap.However,figure 3.3.2(b) shows that if we cut through the active layer,the pumped cavity current will almost not leak out to the active layer of the cold cavity.

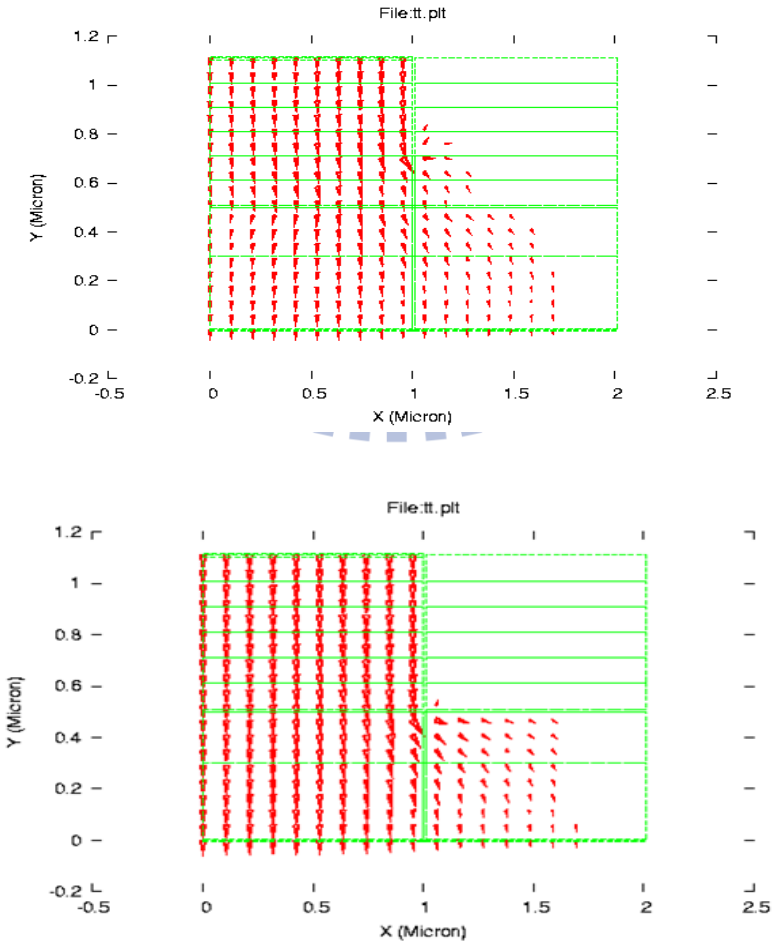

Figure 3.3.2.Current distribution with different depths of the air gap

References

[1] D. C. Byrne, W. H. Guo, Q. Lu and J. F. Donegan “A Tunable Semiconductor Lased Based on Etched Slots Suitable for Monolithic Integration” School of Physics, Trinity College Dublin ,Ireland

[2] N. A. Pikhtin, A. Yu. Leshko, A. V. Lyutetski , V. B. Khalfin, N. V. Shuvalova,Yu. V. Il’in, and I. S. Tarasov “Two-section InGaAsP/InP Fabry-Perot laser with a 12 nm tuning range”, Pis’ma Zh. Tekh. Fiz. 23, 10–15 ~March 26, 1997

[3] H. Hillmer, A. Grabmaier, S. Hansmann, H. -L. Zhu, H. Burkhard, and K. Mazagi, IEEE J. of Selected Topics in Quant. Electr. 1, 356 (1995).

[4]Wan Q, Sun C-Z, Xiong B, Wang J and Luo “A novel multisection distributed feedback laser with varied ridge width for self-pulsation generation” *Chin. Phys. Lett.* 23 2753–5 , (2006)

[5] Larry A. Coldren, and Scott W. Corzine, “ Diode Lasers and Photonic Integrated Circuits”, Wiley Interscience series, New York, (1995).

Chapter4. Experiments Results

4-1. Two-Section Laser Structure

The device is grown on a n^+InP substrate. The one facet is AR(anti-reflection)and the other is HR(high-reflection).There would be an optical feedback light at the HR side traveling through the z-direction cavity. The feedback wavelength is detuning with the original wavelength .The feedback section at HR side becomes a master laser and the other side becomes a slave laser. An air gap is located in the middle section with adjustable width and depth. There would be some optical injection locking phenomenon in the structure. Therefore, we expect that there would be some modification of dynamic characteristics of the laser, such as relative intensity noise(RIN), chirp frequency under these conditions.

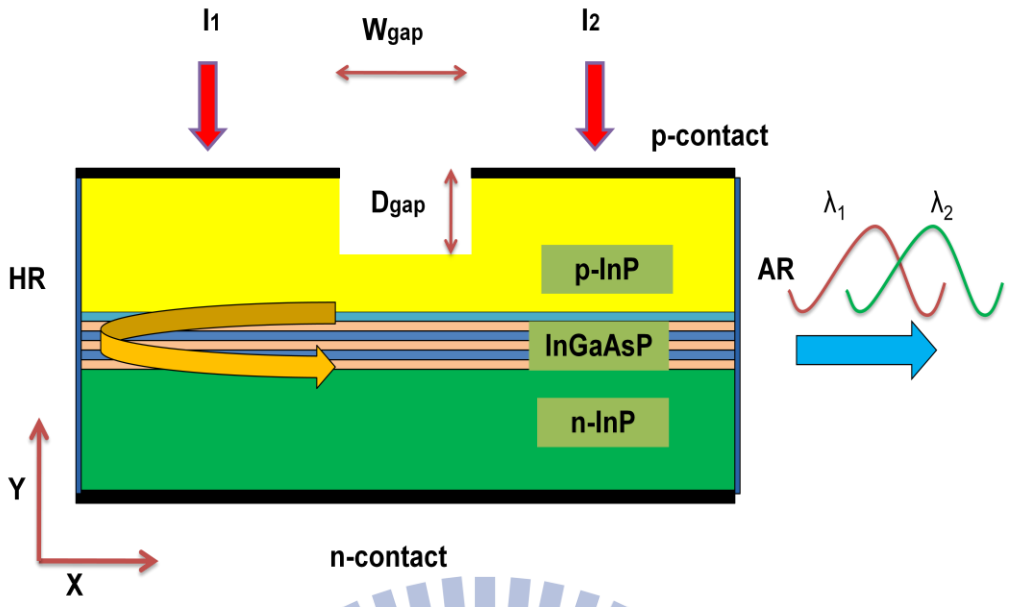

Figure 4.1.1. 1.55μm InGaAsP Fabry-Perot laser with a tunable air gap in the middle section

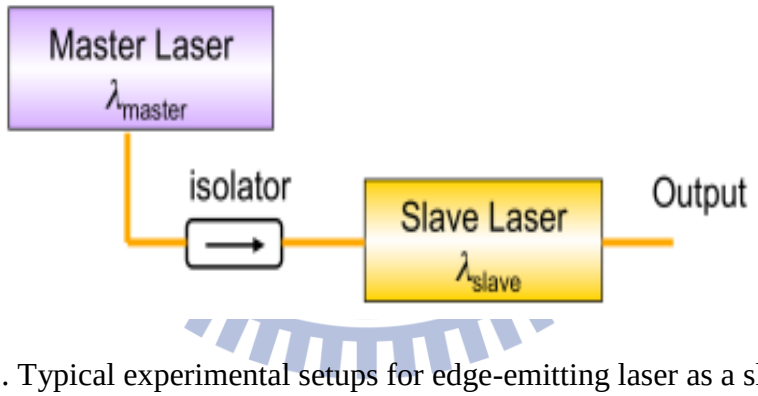

Figure 4.1.2. Typical experimental setups for edge-emitting laser as a slave laser.

4.2 FIB(focus ion beam) Etching Process

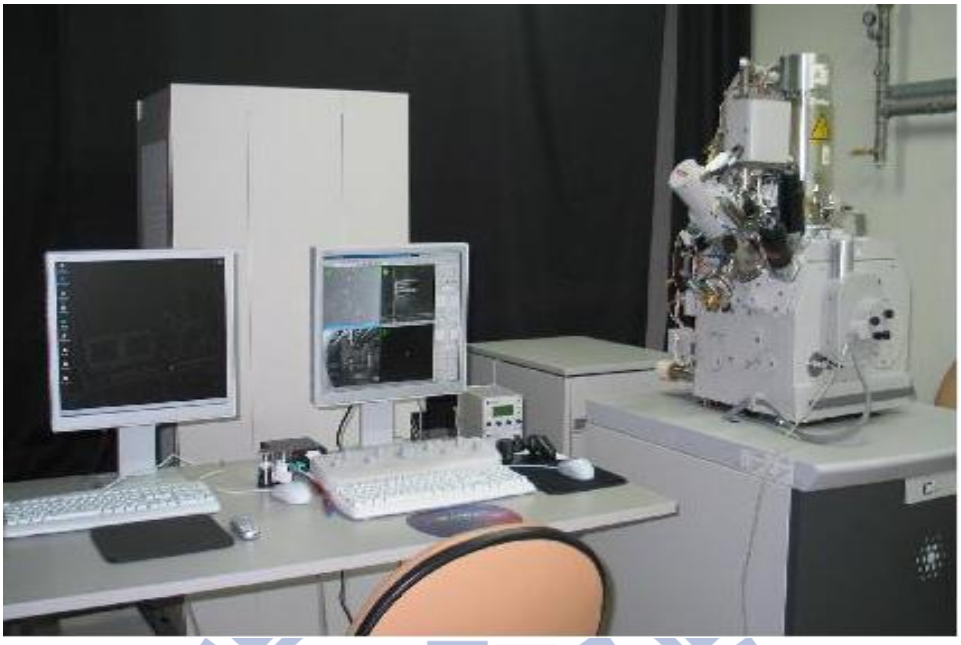

Figure 4.2.1 Dual beam (focused ion beam & electron beam) System (FIB/SEM)

To etch an air gap which we expect in the middle section accurately , we choose the Dual beam (focused ion beam & electron beam) System . Focused ion beam has been widely used for preparing cross-sectional transmission electron microscopy specimens, because of the ease with which a structure having multiple layers of different hardnesses can be etched and the good lateral accuracy. The operating current is about 0.4 nA.If the operating current is too large, the laser device will be damaged.

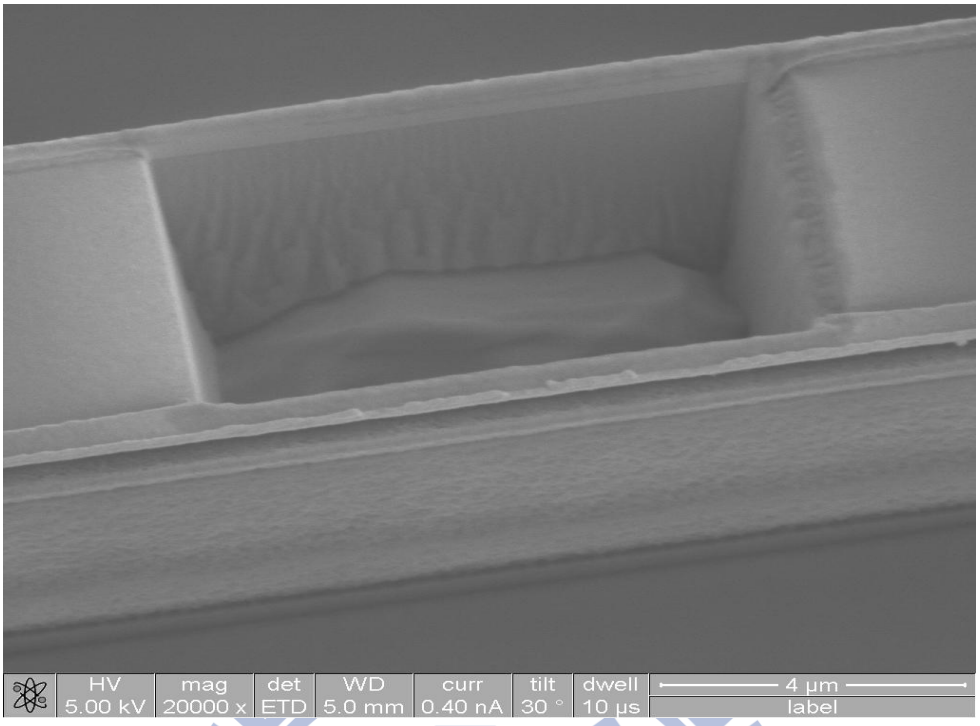

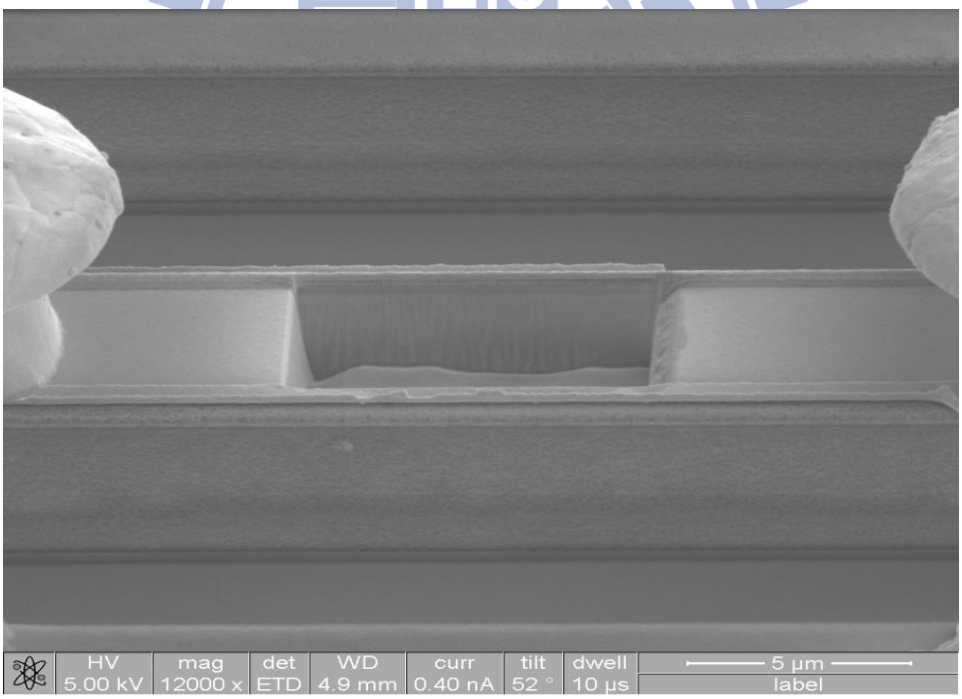

Figure 4.2.2. SEM figure (Dgap is 5um.)

4.3 Leakage Current Measurement

According to the conventional optical injection locking system , there are two independent lasers and other optical devices ,such as isolator and circulator, so the two lasers do not interfere with each other.But,when we make the two independent lasers monolithic two-section laser ,the current distribution in the common laser cavity will redistribute. If the laser is etched to 5um , the resistance between the two electrodes is 168Ω .A more detailed understanding of this relationship can be gained from Fig.4.3.1 and Table 3.

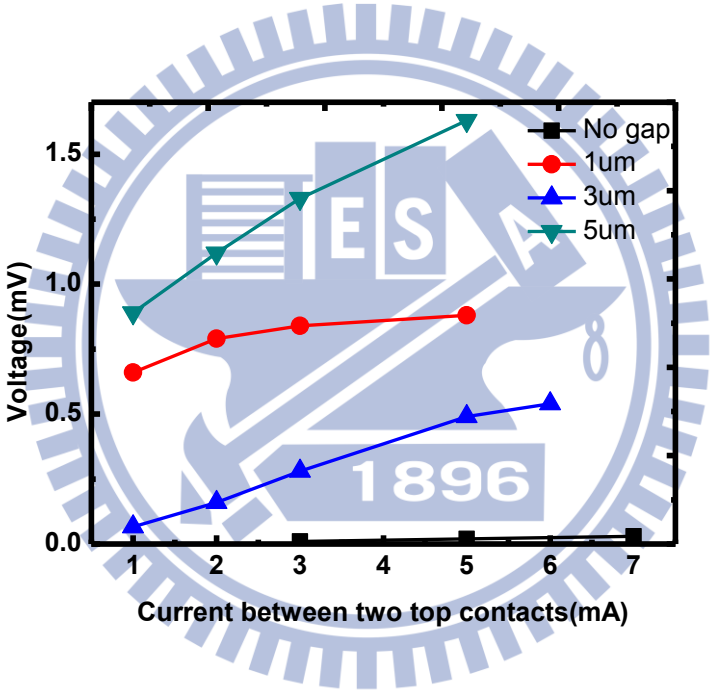

Figure 4.3.1. I-V curve between the two top contacts

Dgap	0um	1um	3um	5um
R(Ω)	4	51	108	168

Table 3.The resistance value between the two top contacts

4.4 Distributed Bragg reflectors on Edge-laser HR facet

4.4.1 Introduction of Distributed Bragg reflectors

Distributed Bragg reflectors (DBRs) served as high reflecting mirror in numerous optoelectronic and photonic devices. It is a periodic structure formed by stacking several pairs of two 1/4-lambda-thick layers with different refractive index. Consider a distributed Bragg reflector consisting of m pairs of two dielectric, lossless materials with high- and low- refractive index n_H and n_L, as shown in Figure 4.4.1. The thickness of the two layers is assumed to be a quarter wave, that is, $L_1 = \lambda_B/4n_H$ and $L_2 = \lambda_B/4n_L$, where the λ_B is the Bragg wavelength.

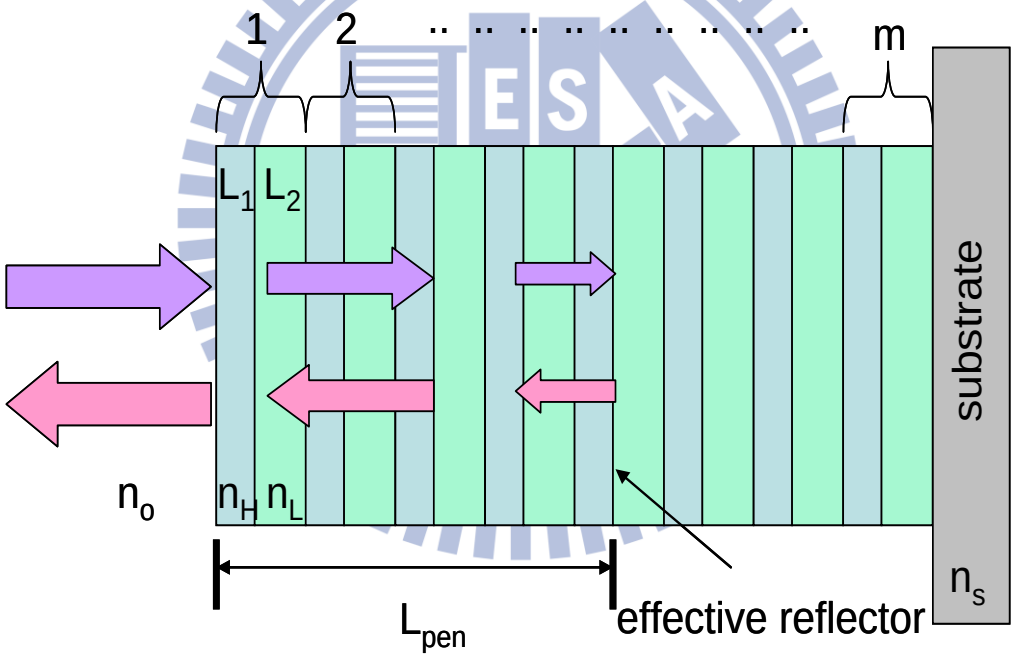

Figure 4.4.1. distributed Bragg reflector

Multiple reflections at the interface of the DBR and constructive interference of the multiple reflected waves increase the reflectivity with increasing number of pairs. The reflectivity has a maximum at the Bragg wavelength λ_B. The reflectivity of a DBR with m quarter wave pairs at the Bragg wavelength is given by

$$R = \left(\frac{1 - \frac{n_s}{n_o}\left(\frac{n_L}{n_H}\right)^{2p}}{1 + \frac{n_s}{n_o}\left(\frac{n_L}{n_H}\right)^{2p}} \right)$$

where the n_o and n_s are the refractive index of incident medium and substrate.

The high-reflectivity or stop band of a DBR depends on the difference in refractive index of the two constituent materials, Δn (n_H - n_L). The spectral width of the stop band is given by

$$\Delta\lambda_{stopband} = \frac{2\lambda_B \Delta n}{\pi n_{eff}}$$

where n_{eff} is the effective refractive index of the mirror. It can be calculated by requiring the same optical path length normal to the layers for the DBR and the effective medium. The effective refractive index is then given by

$$n_{eff} = 2\left(\frac{1}{n_H} + \frac{1}{n_L}\right)^{-1}$$

4.4.2 Reflectance simulation of T_iO_2/SiO_2 DBRs

To determine how many pairs DBRs are required for the laser, the realization of reflectivity spectra of DBR is inevitable and necessary. In the following, we simulate and discuss the reflectance of reflectors we used, TiO_2/SiO_2 DBRs, to understand the DBR pairs we required at least to deposit for a laser facet. Reflectivity spectra of DBR structures here were simulated using the transfer matrix method. The incident angle of illumination and wavelength of the reference light were set to be 0^o (the direction normal to the sample surface) and 1550nm, respectively.

Dielectric mirror has the advantage of the large refractive index contrast between two different dielectric materials so it only needs a few pairs of DBR to form high reflectivity mirror. In most dielectric DBRs, SiO_2 is usually used as the low refractive index material due to its some advantaged characteristics such as relative low refractive index than many other dielectric materials. It is easy and cheap to get, hard to decompose, and high transparent window from the wavelength of 180 nm to 8 μm. As to the high refractive index material, TiO_2 is a proper selection owing to benefits of low absorption and high transparency in IR ray. The refractive index of SiO_2 and TiO_2 at wavelength of 1550 nm, used as the parameters in the simulation, are n_{SiO2} = 1.463 and n_{TiO2} = 2.5. The 8 pairs of TiO_2/SiO_2 mirror can have a high reflectivity of 98% and the wide stop band about 200 nm. Therefore, we use at least 8 pairs of TiO_2/SiO_2 DBR as the mirror in the following experiments.

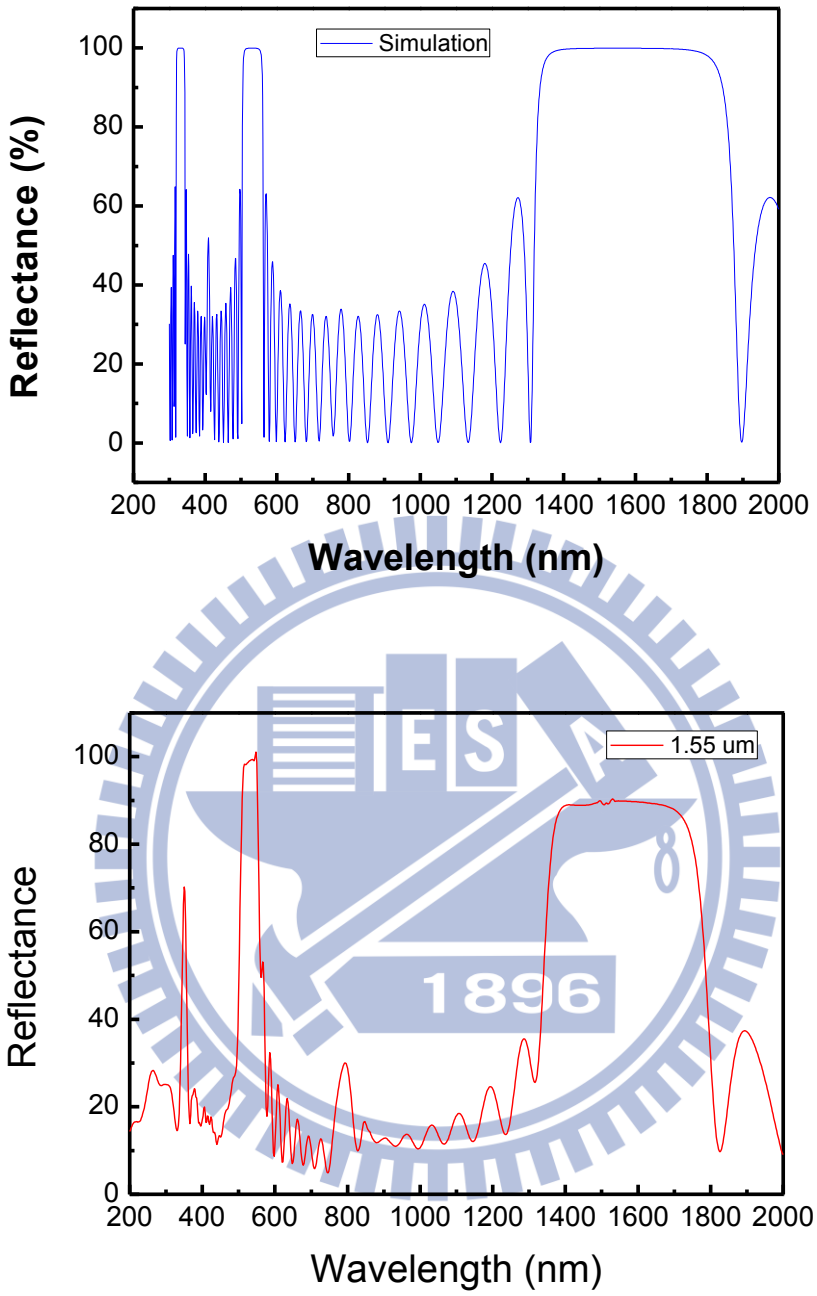

Figure 4.4.2(a) TFCalc simulation for 1.55um(b) reflectivity measurement on the HR facet(200nm~2000nm)

4.5 Optical Spectrum and RF Measurement

4.5.1 Experimental Setup

We setup our system which can test our sample non-packaged device . The scheme of the measurement system, which illustrates in Fig 4.5.1, including two DC power supplies, single-mode fiber, optical spectrum analyzer (OSA, AQ6317B), electrical spectrum analyzer, and semiconductor optical amplifier (SOA).The optical spectrum data were collected using a floppy disk and the RIN data were collected using a GPIB card and Labview software.

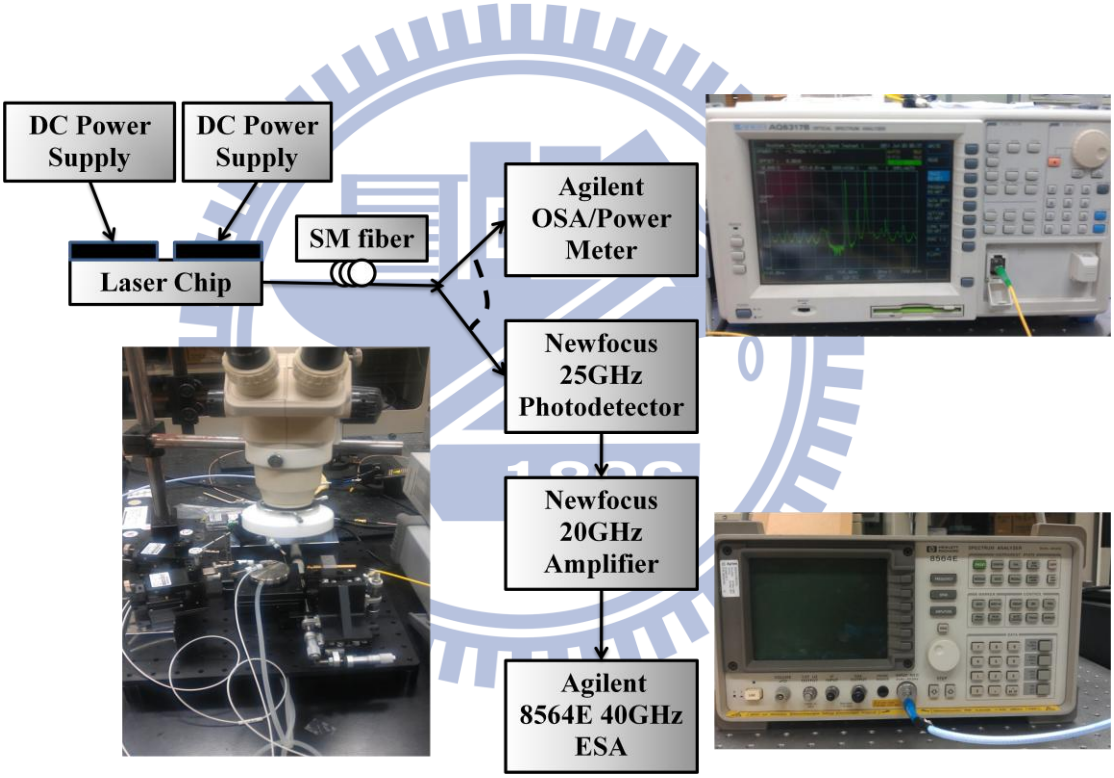

Figure 4.5.1. experimental setup for measurement

4.5.2 Optical Spectrum Measurement Without FIB Process

First of all, before the FIB process , we measure the optical spectrum of the coated lasers and uncoated lasers, which are biased on the slave laser section. These presents that the uncoated lasers have more clearly DFB modes. We choose the coated lasers to do following experiments. In addition, the lasers are dual-modes lasing rather than single-mode lasing. It might because of the asymmetric two laser cavities .

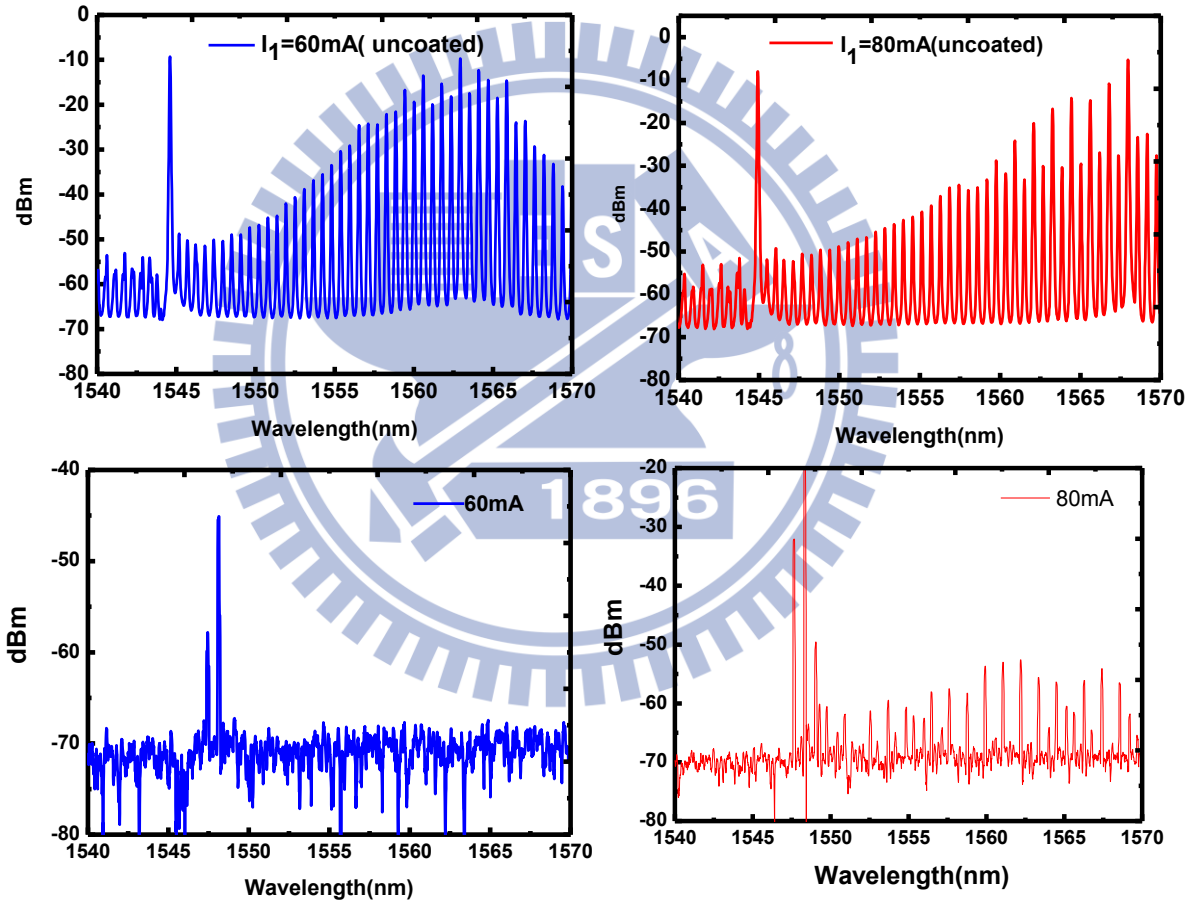

Figure 4.5.2.optical spectrum of two-section laser(a)uncoated at 60mA(b)uncoated at 80mA (c)coated at 60mA (d)coated at 80mA

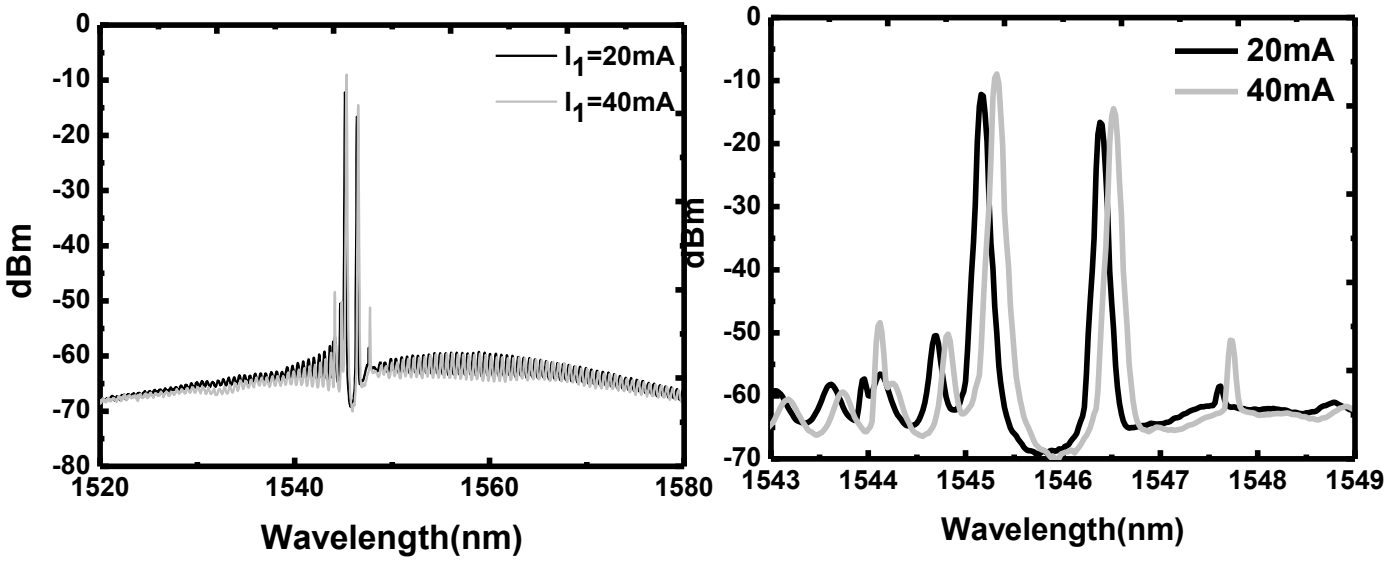

Figure.4.5.3 (a) optical spectrum of the coated and un-FIB laser (b) Zoom in

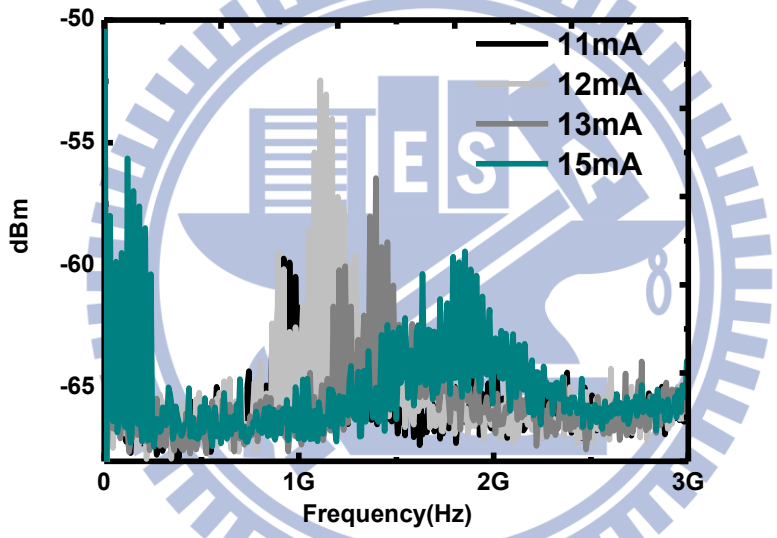

Figure.4.5.4 RIN spectrum of coated and un-FIB two-section laser

Before the FIB process, we have to realize optical spectrum and RF performance clearly. Figure.4.5.3 shows that the two-section laser is not single-mode lasing .One explanation for this is that the two cavities is not independent. The result may be explained by considering the current distribution.Besides,the RIN spectrum presents that the laser shows low relative intensity noise level about -140dB/Hz.

4.5.3 Optical Spectrum Measurement with an air gap

After the FIB process, we measure the optical and RF spectrum. Figure 4.5.5 shows that the slave laser is single-mode lasing with I_2=0mA.A partial explanation for this may lie in the fact that the two-section laser have complete two isolated resonance cavities. The sample has excellent side mode suppression ratio (SMSR) 48.3dB.Besides, the figure 4.5.6 shows that the relaxation frequency increases when the bias current increases. These findings are in accord with the results of the previous studies

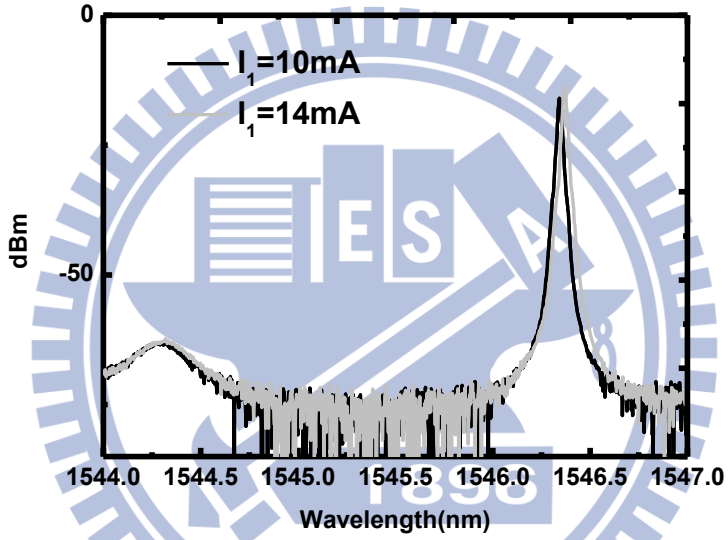

Figure 4.5.5. optical spectrum of the slave laser with an air gap(No injection)

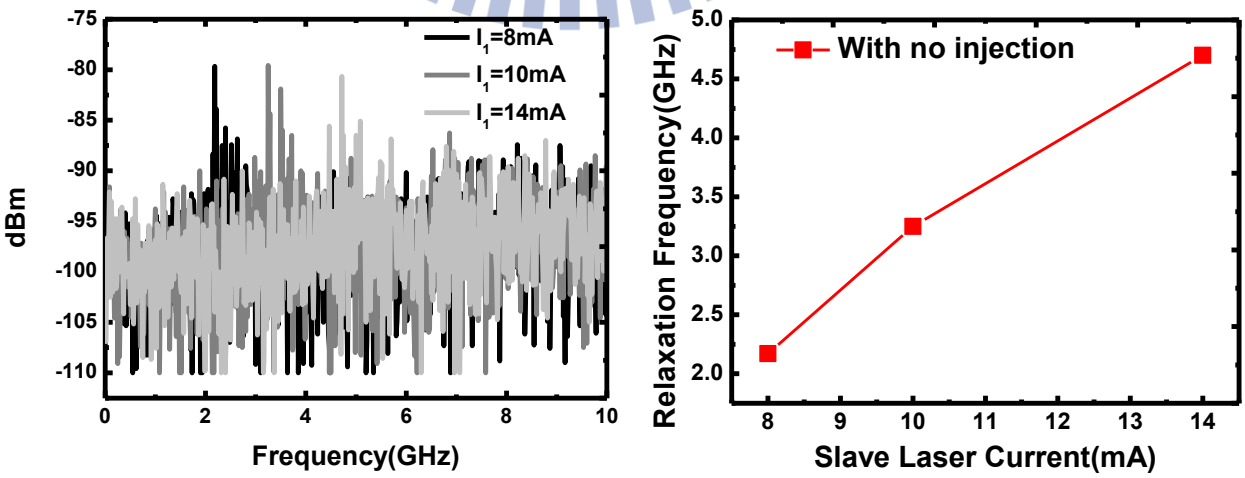

Figure 4.5.6.(a) RIN spectrum of the slave laser with an air gap(b)Relaxation frequency peaks versus the slave laser bias current

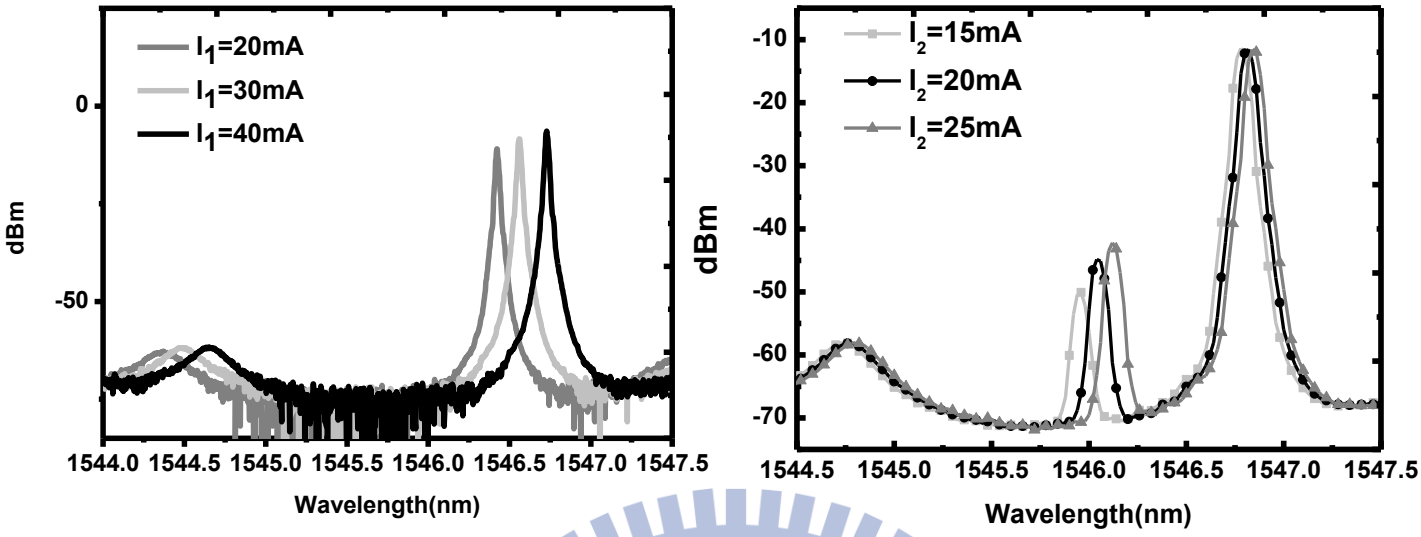

Figure 4.5.7.optical spectrum (a) No injection (b) with weak injection(I_1=30mA)

We start to bias the master laser to measure optical spectrum. Figure 4.5.7.(a) show that the two-section laser is single-mode lasing and red-shift with increasing slave bias current. The more likely explanation rest in the nature of the cavity temperature.When we turn on the master laser and fix the I_1 at 30mA,we can see the red shift in the figure 4.5.7(b).Therefore, we can assure that the moving wavelength is belong to the master laser.Besides,we can calculus the mode spacing and RF frequency in the following table. The RF signal range could be up to 100 GHz level ,but our photodector is only 20 GHz.The mode spacing is in agreement with the corresponding RF frequency according to the following beating fomula:

$$\Delta f_{\det uning} = C \cdot \frac{\Delta \lambda_{\det uning}}{\lambda^2}$$

	I_2=15mA	**I_2=20mA**	**I_2=25mA**
Mode spacing	-0.84nm	-0.78nm	-0.72nm
RF frequency	105.4GHz	97.8GHz	90.35GHz

Table 4.Mode spacing and RF frequency with weak injection

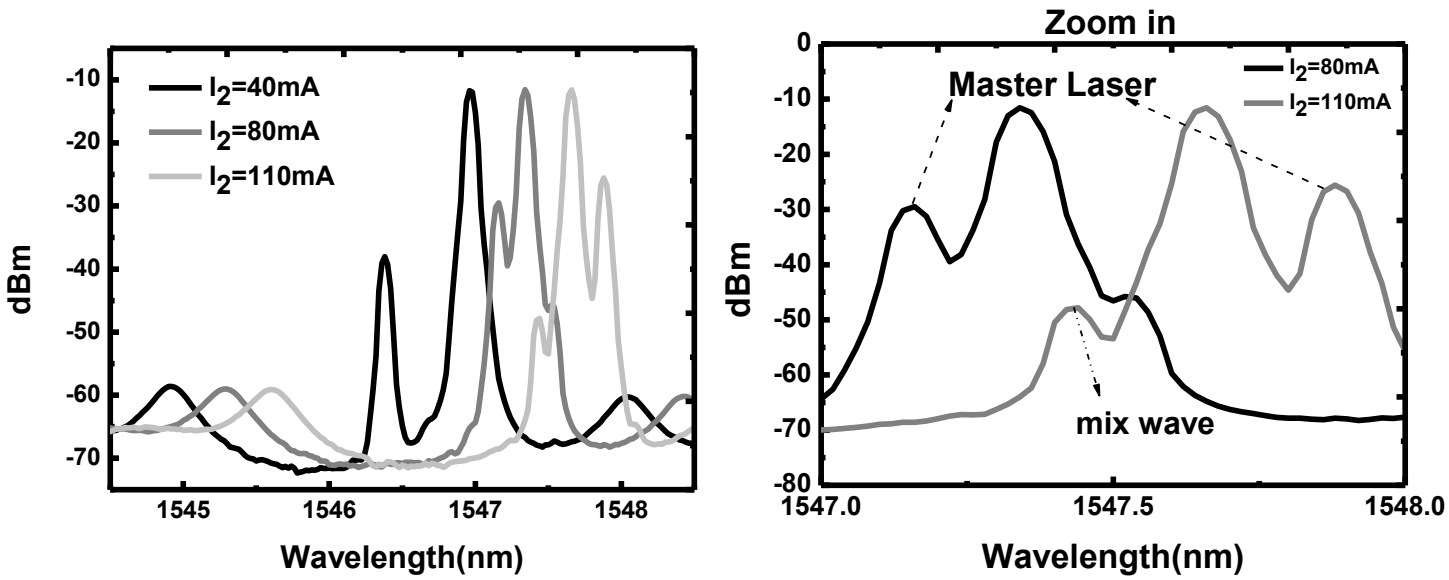

Figure 4.5.8(a)optical spectrum with strong injection(I_1=30mA)(b)Zoom in

	I_2=40mA	I_2=80mA	I_2=110mA
Mode spacing	-0.58nm	-0.21nm	0.22nm
RF frequency	72.7GHz	26.3GHz	28.8GHz

Table 5. Mode spacing and RF frequency with strong injection

The previous literature demonstrates that injection locking happens in a special range.So,the interesting thing which we want to search in these optical spectrums is how to find the injection range. The figure 4.5.8 presents that the λ_{master} is gradually close toλ_{slave} when we increase the I_2 40mA,80mA,110mA.At about I_2=80mA,the locking phenomenon appears. If we increase the current to about 110 mA,theλ_{master} will exceed theλ_{slave}.In other words, the locking range is located in I_2=80~110 mA.

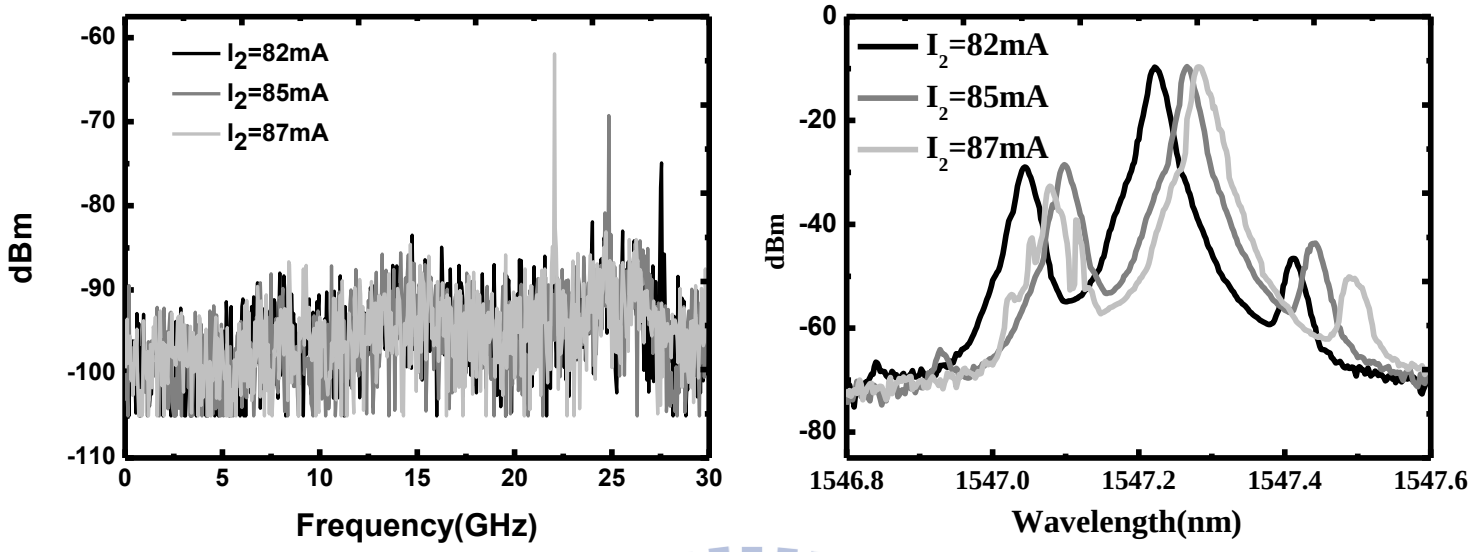

Figure 4.5.9 optical spectrum and RIN spectrum of the injection-locked laser with strong injection at 82mA~87mA(I_1=30mA)

	I_2=82mA	I_2=85mA	I_2=87mA
Mode spacing	0.21/-0.21 nm	0.2/-0.2 nm	0.17/-0.17 nm
RF frequency	27GHz	25GHz	22.5GHz

Table 6. Mode spacing and RF frequency of the injection-locked laser with strong injection at I_2=82mA~87mA

Once we find out the injection locking range, we have to tune finely from I_2 80mA to 110mA.However,because our current is not stable enough, so the current tuning spacing is 2mA~3mA.Figure 4.5.9 presents the relation between RIN spectrum and optical spectrum. If we fix the I_1 30mA and increase the current from 82 mA to 87 mA,the relaxation frequency is 27 GHz to 22.5 GHz as observed in Table 6.

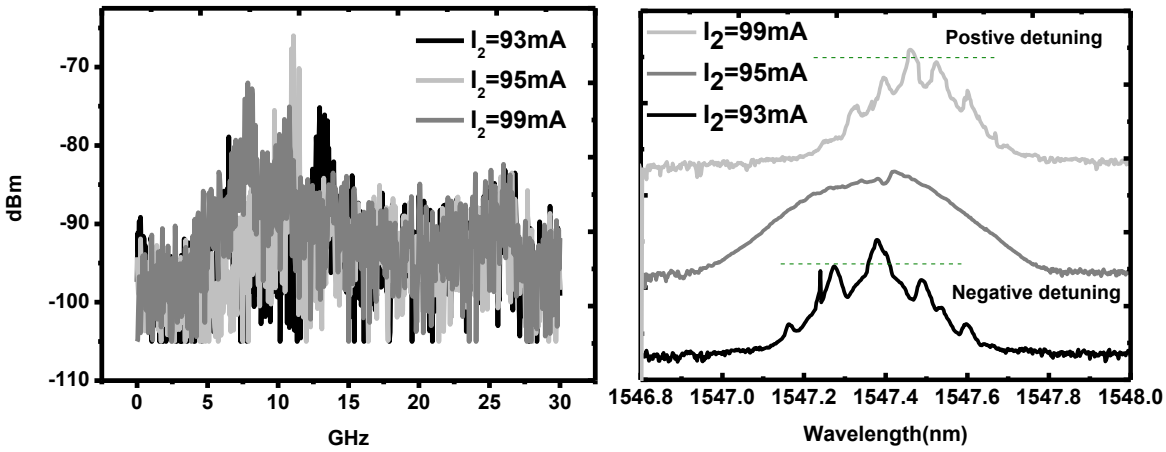

Figure 4.5.10 optical spectrum and RIN spectrum of the injection-locked laser with strong injection at 93mA~99mA(I_1=30mA)

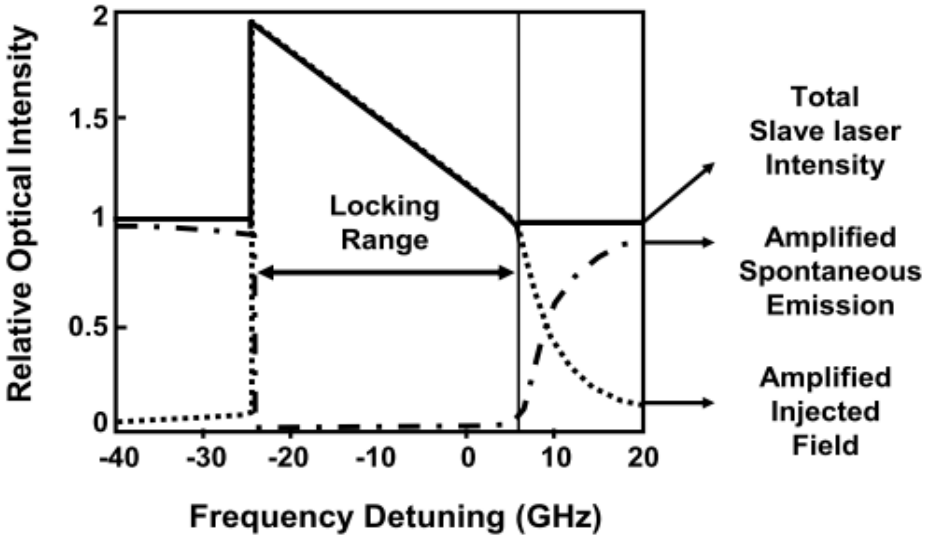

Figure 4.5.11. Locking range and stability of injection locked 1.54 μm InGaAsP semiconductor lasers [1]

However, when we increase bias current I_2 from 93mA to 99mA,there are some important things shown as Figure 4.5.10.First,at 93mA the detuning wavelength is still negative, but at 95mA the linewidth becomes very wide and the RIN spectrum becomes very noisy. The wavelength detuning becomes positive until the bias current is 99 mA.The RIN level is about -131.8dB/Hz ~ -125dB/Hz.

All of the measures were strongly positively correlated. Because of the optical power degrading at 91mA ,the injection ration gradually decreases with I_2=93mA to 99mA .Besides, negative detuning turn to postive detuning is under the bias current range. Once the injection ratio fall down, the spontaneous emission is increase.These results are correspond to the Figure 4.5.11[1]. Therefore,the linewidth will be larger and the noise level will increase more.

Figure 4.5.12 presents that theλ_{slave} peaks versus I_1 without ML injection and λ_{master} peaks versus I_2 with fixed I_1.The figure demonstrates that bias current leads to laser current increasing and the red-shift. Figure 4.5.13 demonstrate that the relaxation frequency under injection locking range is from 7 GHz to 27 GHz.

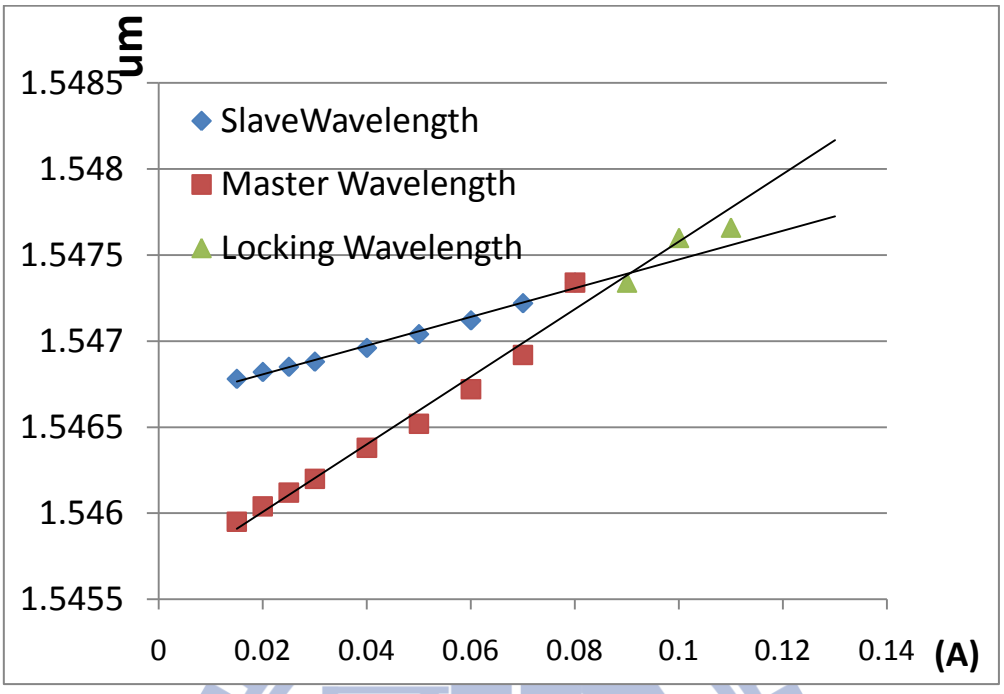

Figure 4.5.12 Optical Spectrum Analysis

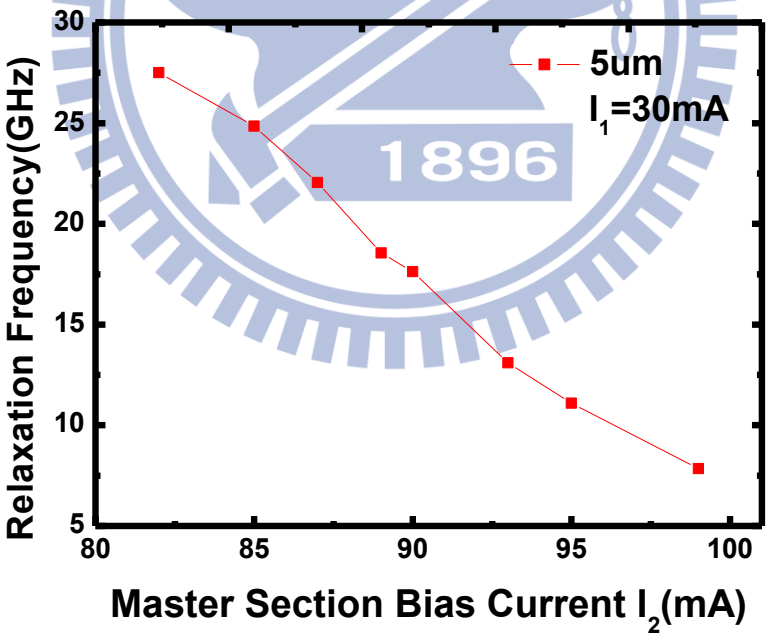

Figure 4.5.13 Relaxation frequency versus I_2 with fixed I_1

Reference

[1] C. H. Henry, N. A. Olsson, and N. K. Dutta, "Locking range and stability of injection locked 1.54 μm InGaAsP semiconductor lasers", IEEE J. Quantum Electron., vol. 21, no. 8, pp. 1152-1156, Aug. 1985

Chapter 5.Conclusion

We have demonstrated a simple method for optical generation of millimeter wave using a single chip laser without other external optical devices. By adjusting moderately bias currents on each section without modulation , by means of self-feedback pulsation we can have an environmentally robust and simple injection locking system. A signification improvement in relaxation frequency was obtained. The relaxation frequency can be enhanced to 27 GHz under some injection condition by optical injection locking technique with different air D_{gap} from RF measurements. It should be noted that frequencies beyond 27 GHz, which is the limit of the RF-measuring system, are estimated by the modes spacing in the optical spectra. Thesis data lend support to our idea. While research on these questions is still at a beginning stage, findings will have broad implications in a number of areas. Future research is obviously required, but this is an exciting first step.